CRYSTAL GROWTH & DESIGN

Article

pubs.acs.org/crystal

Charge Density Analysis and Topological Properties of Hal_3-Synthons and Their Comparison with Competing Hydrogen Bonds

Mariya E. Brezgunova,[†,‡] Emmanuel Aubert,[†,‡] Slimane Dahaoui,[†,‡] Pierre Fertey,[§] Sébastien Lebègue,[†,‡] Christian Jelsch,[†,‡] János G. Ángyán,[†,‡] and Enrique Espinosa*[,†,‡]

[†]Université de Lorraine, CRM[2], UMR 7036, Institut Jean Barriol, 54506 Vandoeuvre-lès-Nancy, France

[‡]CNRS, CRM[2], UMR 7036, 54506 Vandoeuvre-lès-Nancy, France

[§]Synchrotron Soleil, L'Orme des Merisiers Saint-Aubin, BP 48, 91192 Gif-sur-Yvette, France

Supporting Information

ABSTRACT: Trimers based on intermolecular halogen-bonding interactions (Hal_3-synthons) have been studied in hexachlorobenzene, hexabromobenzene, pentachlorophenol, and pentabromophenol. Attention is paid to the comparison of Cl_3- and Br_3-synthons and to their competition with hydrogen bonds (HBs), based on the experimental and theoretical charge density analyses in crystal and gas phases. The main differences between Cl_3- and Br_3-synthons are established coming from the particular structure of the valence shell charge concentration region in Cl and Br atoms. Electrophilic−nucleophilic interactions take place within the intermolecular regions of Hal_3-synthons by putting face-to-face charge depletion (CD) and charge concentration (CC) regions belonging to the valence shell of the halogen atoms. The electrostatic interaction follows the electrophilic and nucleophilic power of these regions and is monitored by the negative Laplacian values normalized to charge density unit (L/ρ) at the corresponding topological critical points (CPs) of the $L(\mathbf{r}) = -\nabla^2\rho(\mathbf{r})$ function. According to the topological and energetic properties at CPs of $\rho(\mathbf{r})$ and $L(\mathbf{r})$, it is observed that Hal_3-synthons can successfully compete with intermolecular HBs in the analyzed structures. On the basis of the estimated interaction energy and the electrostatic descriptor $\Delta(L/\rho) = (L/\rho)_{CC} - (L/\rho)_{CD}$, we conclude that a strong dispersion contribution assists Hal3-synthons in this competition.

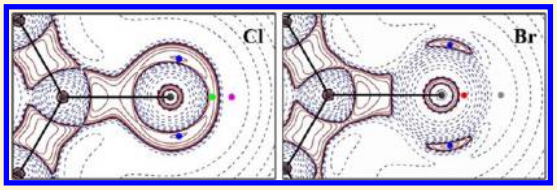

INTRODUCTION

Although halogen bonding has been known for many years in crystal engineering,[1] it is still the subject of intense research efforts.[2] It describes a directional, stabilizing, noncovalent interaction that occurs between halogen atoms (Hal···Hal) or between a halogen atom and a Lewis base (Hal···B). Halogen bonding exhibits many similarities with hydrogen bonding (HB),[3] with which it can even successfully compete.[4]

Considering that the halogen atom (Hal) and the halogen bond electron donor (Hal or Lewis base) are supposed to be partially negatively charged, the very existence of the halogen bond is, at first sight, puzzling. This effect was explained by the anisotropic nature of the electron density, $\rho(\mathbf{r})$, around the halogen nucleus, leading to a larger atomic radius in the equatorial region and a smaller atomic radius along the polar direction. As a consequence, these regions exhibit concomitant negative and positive electrostatic potential magnitudes,[5] and then the halogen atom behaves as a nucleophile at the equator and as an electrophile along the pole direction (Scheme 1a).[6] The anisotropic distribution of $\rho(\mathbf{r})$, called "polar flattening", explains why the nature and the strength of the Hal···Hal interaction strongly depend on its geometry.

According to earlier studies,[7] there are two distinct types of angular preferences for C−X_1···X_2−C (X = halogen) interactions, as depicted in Scheme 1b,c. The first arrangement (type-I) occurs when $\theta_1 \approx \theta_2$, where θ_1 and θ_2 are the C−X_1···X_2 and X_1···X_2−C angles, respectively. The second geometry (type-II) arises when $\theta_1 \approx 90°$ and $\theta_2 \approx 180°$. Among type-I and type-II geometries, the former is believed to be a consequence of close packing, whereas the latter is described as a polarization-induced contact stabilized by the electrostatic forces.[8]

A particular geometrical case of Hal···Hal interactions concerns the recurrent structural motifs formed by the association of three halogen atoms (Scheme 1d), called synthons. It should be marked that triangular Hal_3-synthons appear as important intermolecular building units used for structure design. Originally, the cooperative effect in Hal_3-synthons, enhancing the strength of the Hal···Hal interaction, was noticed by Desiraju and co-workers in 1998.[9] Shortly after, Mak et al. examined the interactions for a series of tris(bromoaryl)triazines and showed how the Br_3 supramolecular synthon could be effectively utilized in the construction of host frameworks.[10] Bosch and Barnes explored the molecular packing in the crystal structure of trihalomesitylenes (Hal = Br, I) and concluded that the donor−acceptor Hal···Hal interactions must be considered as viable driving forces for making synthons to be used in crystal

Received: July 13, 2012
Revised: September 28, 2012
Published: October 3, 2012

   dx.doi.org/10.1021/cg300978x | *Cryst. Growth Des.* 2012, 12, 5373−5386

Scheme 1. (a) Anisotropic Distribution of $\rho(r)$ around Halogen Atom (X), Showing Different Atomic Radii (r_{min}/r_{max}) along Polar and Equatorial Directions, (b) Type-I Interaction ($\theta_1 \approx \theta_2$), (c) Type-II Interaction ($\theta_1 \approx 90°$, $\theta_2 \approx 180°$), and (d) Hal_3-Synthon Type Interaction ($\theta_1 \approx 120°$, $\theta_2 \approx 180°$)

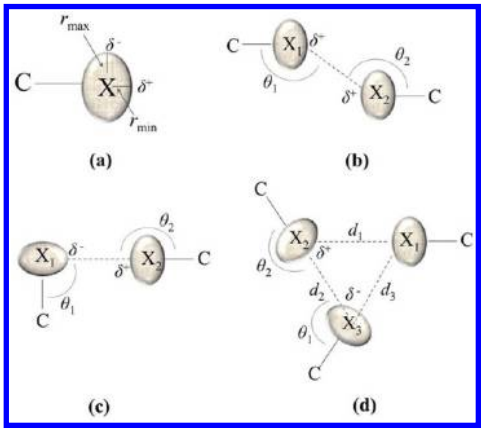

engineering.[11] In a more recent work, Nangia and co-workers have reported that the persistent crystallization of 2,4,6-tris-(4-halophenoxy)-1,3,5-triazine host molecules via the Hal_3-synthon (Hal = Cl, Br, or I) underscores the stability of this cyclic cooperative array for assembling host frameworks.[12]

From the geometries of Hal_3-synthons, it is easily anticipated that the relative positions of electrophilic and nucleophilic sites within these structural motifs are close to those formed in type-II interactions. Thus, a polar δ^+ region of one halogen atom points toward the equatorial δ^- region of an adjacent one in such a way that halogen atoms behave as donor and acceptor. As a result, the bonding picture of Hal_3-synthons is mainly achieved by electrostatics,[12,13] where cooperative contributions add to a gain in stabilization.[14] This has been recently revealed within a Cl_3-synthon by performing the experimental electron density analysis of the crystal structure of C_6Cl_6,[15] from which type-II interactions in the Cl_3-synthon were characterized as electrophilic−nucleophilic in nature, involving oppositely polarized regions ($Cl^{\delta+}\cdots Cl^{\delta-}$) in front of each other. As a consequence, type-II interaction was understood as attractive, corresponding to the Williams model.[16]

Concluding that trimers based on Hal_3 interactions behave as structure-determining synthons in many investigated systems, it is then of special importance to investigate the established electrophilic−nucleophilic interactions by characterizing the trends appearing for each Hal_3-synthon (Hal = Cl, Br). To this end, we focus our attention on the comparison of the Cl_3- and Br_3-synthons as derived from the X-ray multipole-refined electron density and from density functional theory (DFT) calculations. Here, we present the crystal structures and charge density models of hexachlorobenzene (C_6Cl_6) discussed earlier,[15,17] and the isostructural hexabromobenzene (C_6Br_6), along with these of pentachlorophenol (C_6Cl_5OH) and pentabromophenol (C_6Br_5OH) (Scheme 2). The very similar intermolecular interactions found between these bromine- and chlorine-containing crystal structures permit a straightforward comparison of Cl_3- and Br_3-synthons. The electrostatic contribution to the type-II interaction strength is one of the focused subjects in this work, being measured from the nucleophilic and electrophilic power of the regions facing each other in Hal_3-synthons (Scheme 1d).

Scheme 2. Molecular Diagrams of (a) C_6Cl_6, (b) C_6Br_6, (c) C_6Cl_5OH, and (d) C_6Br_5OH

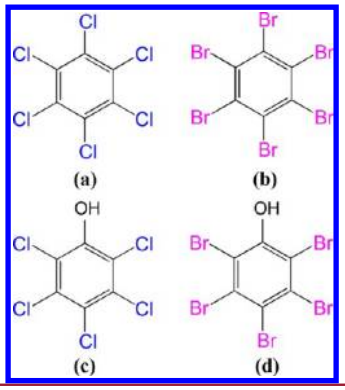

Nowadays, charge density analysis[18] based on experimental measurements and periodic theoretical calculations[17] have reached a stage where parameters, derived from both the electron density distribution $\rho(\mathbf{r})$ and its topology, allow obtaining the electron properties that characterize the features associated with chemical bonding and intermolecular interactions. Thus, the analysis of $\rho(\mathbf{r})$ in these crystal structures provides a quantitative basis to characterize Hal_3-synthons and their interaction strengths.

EXPERIMENTAL AND THEORETICAL METHODS

Crystal Growth. The powders of the four investigated compounds were purchased from Aldrich. Single crystals were obtained by the sublimation method. A raw material in a vacuum-sealed Pyrex glass tube was placed in a bithermal electric furnace with the temperature gradient of 1 °C. The temperature in the furnace was slowly increased (5−10 °C/day) until the formation of the first crystal seeds, when the material was sublimated and its vapor was recondensed in a low-temperature area. Next, this observed temperature was kept constant (50 °C for C_6Cl_6, 110 °C for C_6Br_6, 55 °C for C_6Cl_5OH, and 80 °C for C_6Br_5OH) during several days for a desired crystal growth.

Experimental Details of X-ray Diffraction. Table 1 gathers crystallographic data and experimental details for the crystal structures of C_6Br_6, C_6Cl_5OH, and C_6Br_5OH, while data for C_6Cl_6 can be found in previous works (see Introduction). Data collection strategy and data reduction were carried out with the CrysAlisPro CCD/RED and the DENZO packages.[19] After absorption correction,[20] the measured reflections were sorted, scaled and merged by using the SORTAV program.[21] The structures were solved with SIR92[22] and refined with the SHELXL-97[23] program (WinGX software package[24]). The final crystal structures were obtained after multipolar refinement (based on F), performed with the MoPro program[25] (see CIF files). The packing diagrams were generated using the Mercury 2.3 package.[26] For data collection and structure refinement details, see the Supporting Information.

The experiments were carried out using laboratory Mo Kα radiation source (λ = 0.71073 Å) for C_6Cl_6, C_6Cl_5OH, and C_6Br_5OH. Despite the high absorption coefficient for C_6Br_5OH (μ (Mo Kα) = 21 mm^{-1}), absorption effects were nicely corrected. To reduce the significant absorption effects observed for C_6Br_6 with the same source (μ (Mo Kα) = 24 mm^{-1}), synchrotron radiation (λ = 0.45741 Å) was used (μ = 7.4 mm^{-1}). Nevertheless, the experimental data set for C_6Br_6 proved to be of relatively low quality for charge density analysis (see residuals in Figure S2 in the Supporting Information). Therefore, the experimental multipolar data set was used for structural determination only.

Computational Electron Density. According to previous results,[17] periodic theoretical calculations can be used to resolve complicated experimental situations, such as the C_6Br_6 case, as they can nicely approach experimental electron density determination. Hence, ab initio periodic calculations using DFT have been performed on the crystal structure of C_6Br_6 with the Vienna Ab initio Simulation Package (VASP).[27] The all-electron, frozen core PAW (Projector Augmented Wave) method[28] was applied with the PBE exchange-correlation

dx.doi.org/10.1021/cg300978x | Cryst. Growth Des. 2012, 12, 5373−5386

Table 1. Crystallographic Data and Experimental Details for the Crystal Structures of C_6Br_6, C_6Cl_5OH, and C_6Br_5OH

ID	C_6Br_6	C_6Cl_5OH	C_6Br_5OH
Crystal Structure			
formula weight (g/mol)	551.49	266.33	488.59
temperature (K)	100	100	100
source/wavelength (Å)	synchrotron/ 0.45741	Mo K_α/ 0.71073	Mo K_α/ 0.71073
crystal system/space group	monoclinic/ $P2_1/n$	monoclinic/ $C2/c$	monoclinic/ $P2_1$
unit cell dimensions: a (Å)	8.3000(1)	29.1212(5)	8.1997(5)
b (Å)	3.9332(1)	4.8906(1)	3.9469(3)
c (Å)	15.2342(1)	12.0702(2)	14.8097(10)
β (deg)	92.908(5)	93.775(2)	95.152(6)
volume (Å^3), Z	496.69(2), 2	1715.39(6), 8	477.35(4), 2
calculated density (g/cm^3)	3.688	2.063	3.399
absorption coefficient μ (mm^{-1})	7.42	1.63	20.99
crystal size (mm^3)	0.15 × 0.10 × 0.04	0.16 × 0.13 × 0.05	0.29 × 0.06 × 0.04
F(000)	492	1040	440
Data Collection			
θ_{max} (deg)	27.22	45.44	45.37
$(\sin\theta/\lambda)_{max}$ (Å^{-1})	1.0	1.0	1.0
index range	$-16 \le h \le 16$	$-58 \le h \le 58$	$-16 \le h \le 16$
	$-7 \le k \le 7$	$-9 \le k \le 9$	$-7 \le k \le 7$
	$-30 \le l \le 30$	$-24 \le l \le 24$	$-29 \le l \le 29$
reflections collected	350 604	113 464	26 246
independent reflections	4072	7028	7964
R_{int}	0.0622	0.0381	0.0440
completeness to $(\sin\theta/\lambda)_{max}$ (%)	97.9	97.2	99.3
absorption correction	face analysis	face analysis	face analysis
min/max transmission	0.53/0.75	0.78/0.92	0.07/0.54
Multipolar Refinement Data[a]			
refinement method	F	F	F
reflections number: $I > 3\sigma(I)$/total	4015/4159	5815	6412
GOF on F	1.145/0.069[b]	1.093	0.974
$R(F)$	0.016/0.084	0.013	0.031
$wR(F)$	0.026/0.041	0.011	0.027
$N_{ref}/N_{var.}$	21.1/30.8	15.4	17.0

[a]First and second values for C_6Br_6 correspond to experimental and theoretical (VASP calculations) data. [b]Low goodness-of-fit for C_6Br_6 (theoretical calculations) is due to the use of theoretical structure factors, for which the associated standard deviations are set to 1. In that case, the goodness-of-fit should go to 0 rather than to 1 at the convergence.

functional,[29] using a high (900 eV) plane wave cutoff and a dense (8, 14, 4) k-point mesh to ensure convergence. Further computational details can be found in the Supporting Information.

In addition to the C_6Br_6 periodic calculations, gas-phase optimizations have been carried out for C_6Cl_6, C_6Cl_5OH, C_6Br_5OH, and C_6Br_6 molecules at the Møller−Plesset second-order level of theory using the Gaussian09 program package.[30] All electrons were included in the correlation calculation, and the aug-cc-pVTZ basis set was employed for all atoms. The topological analysis of the Laplacian of the electron density on the converged structures and the corresponding maps was performed with the AIMAll code.[31]

Multipolar Refinement. To analyze the electron density distribution $\rho(\mathbf{r})$ in the crystal phases of the studied compounds, the Hansen−Coppens[32] model has been fitted against either experimental or theoretical structure factors. The choice of the parameters (ξ, n_l) of the Slater-type functions was based on the electron density experimental studies performed earlier (see Table S1 in the Supporting Information).[33] The multipolar refinements were performed with the MoPro program.[25] The multipolar charge density parameters were refined according to a strategy previously proposed.[25a] Initial κ and κ' parameters for hydrogen atoms were set to 1.16 instead of 1, as this chemical species is expected to be electron depleted in the intermolecular region and the electron density is therefore contracted toward the nucleus.[34] The most appropriate value of standard deviation for restraints (σ_{sym} = 0.02) was found from R_{free} calculations.[35] The residual electron density maps show randomly distributed electron density, not exceeding 0.2 e Å^{-3} for chlorine and 0.3 e Å^{-3} for bromine compounds up to a resolution of 0.9 Å^{-1} (see Figure S1 in the Supporting Information). The good quality of the multipolar models was as well validated by the low values of the rigid bond test,[36] performed at convergence.

Topological Analysis of $\rho(\mathbf{r})$ and $L(\mathbf{r})$ Functions. Within the framework of the QTAIM, the topologies of $\rho(\mathbf{r})$ and its negative Laplacian, $L(\mathbf{r}) = -\nabla^2\rho(\mathbf{r})$, permit to extract significant information on bonding interactions[37] and molecular crystals.[38] In addition to the topological properties of $\rho(\mathbf{r})$ at bond critical points (CPs), experimental estimations of local energetic properties at the same points[39−41] are also used to characterize interactions in Hal_3-synthons (see the Supporting Information for detailed description).

The topological analysis of $L(\mathbf{r}) = -\nabla^2\rho(\mathbf{r})$ function permits to point out charge depletion and charge concentration regions that are associated with the electrophilic and nucleophilic sites in the outer valence shell region of an atom.[17,37] Thus, on the basis of the complementarity between electron distributions,[37] which states that local maxima and local minima of $L(\mathbf{r})$ in different molecules combine to each other, we have characterized electrophilic−nucleophilic interactions from preferred directions of molecular alignment in Hal_3-synthons and HBs.

RESULTS AND DISCUSSION

Crystal Structures Description. The crystal structures of C_6Cl_6, C_6Br_6, C_6Cl_5OH, and C_6Br_5OH were previously determined by several groups.[42−47] Thus, C_6Cl_6 crystallizes in the monoclinic system (space group $P2_1/n$)[42] and was found to be isostructural with C_6Br_6,[43] firstly determined by neutron powder diffraction at 300 K.

While only one phase was observed for the isostructural C_6Cl_6 and C_6Br_6 compounds, the structures of C_6Cl_5OH and C_6Br_5OH were found to crystallize in two polymorphic phases, which are referred here as low- and high-temperature (LT and HT) phases. Indeed, investigating the thermodynamic behavior of C_6Cl_5OH and C_6Br_5OH, Wójcik et al.[44] observed that these compounds exhibit a first-order phase transition at 341 and 441.5 K, respectively. The crystal structure of the C_6Cl_5OH LT phase was solved by combining nuclear quadrupole resonance and X-ray diffraction data at room temperature[45] (monoclinic system, $C2/c$ space group, Z = 8, unit cell parameters: a = 29.11(3) Å, b = 4.93(5) Å, c = 12.09(2) Å, β = 93.38(4)°, V = 1732(5) Å^3). The crystal structure of its HT phase was as well determined at room temperature. Indeed, while cooling, the HT phase remains for several hours as a metastable state, allowing the structure determination, until the stable LT phase is reconstructed. This allowed Wójcik and Rohleder[46] to conclude that the HT phase of C_6Cl_5OH, crystallizing in the monoclinic system, $P2_1$ space group, has structural synthons similar to those observed in C_6Cl_6.[42]

In contrast to C_6Cl_5OH, the C_6Br_5OH phase transition at 441.5 K is not reversible on cooling, and its HT phase has not been determined so far. The LT phase of C_6Br_5OH, determined by Betz et al. at 200(2) K,[47] was found to crystallize in the monoclinic system, $C2/c$ space group (Z = 8, unit cell parameters: a = 32.3058(15) Å, b = 3.9957(2) Å, c = 16.1887(8) Å, β = 112.118(3)°, V = 1935.93(17) Å^3). On the other hand, Wójcik et al.[44] determined the C_6Br_5OH crystal structure at room temperature in the monoclinic system, $P2_1$ space group (with

dx.doi.org/10.1021/cg300978x | Cryst. Growth Des. 2012, 12, 5373−5386

$Z = 2$ and unit cell parameters: $a = 8.238(8)$ Å, $b = 4.021(9)$ Å, $c = 14.822(8)$ Å, $\beta = 95.82(6)°$), being similar to that of C_6Br_6[43] and forming molecular arrangements analogous to those found in the HT phase of C_6Cl_5OH and C_6Cl_6. Probably, the existence of two C_6Br_5OH forms, both at low temperature conditions, is induced by the crystallization method. The crystals of the $C2/c$ phase were obtained upon recrystallization of the compound from boiling toluene, while for the $P2_1$ phase, the C_6Br_5OH single crystals were obtained by slow evaporation from a benzene solution.

In all of the mentioned OH-containing crystal structures, the molecules are linked by infinite monodimensional chains of hydrogen bonds with shorter O···O distances in the case of both C_6Br_5OH crystal forms (2.97 Å for C_6Cl_5OH and 2.84/2.88 Å for C_6Br_5OH structures).[44,45,47] Besides, the OH-groups in the studied structures take part in additional interactions. A bifurcated interaction involving a hydrogen bond and a contact between an adjacent oxygen atom and a halogen atom in *ortho*-position as acceptors was observed in the case of the LT phase of C_6Cl_5OH (O−H···O = 2.97 Å and O···Cl = 3.28 Å),[45] in contrast to the C_6Br_5OH phases where these intermolecular contacts were not indicated. The existence of an intramolecular O−H···Br contact was observed in both C_6Br_5OH structures (the H···Br distance being 2.29 and 2.48 Å for the $P2_1$ and $C2/c$ phases, respectively).[44,47]

From the IR spectra of the LT and HT phases of C_6Cl_5OH and C_6Br_5OH,[44] it was shown that the phase transition is associated with the breaking of the intermolecular hydrogen bond and the proceeding reorientation of the molecules. Moreover, in comparison with the C_6Cl_5OH structure, the higher phase transition temperature of C_6Br_5OH was explained by its higher crystal density, which correlates with stronger intermolecular forces (also supported by shorter O···O distances) and the occurrence of an intramolecular O−H···Br interaction. The broadening of the OH band in the HT phase of C_6Br_5OH indicates that the later intramolecular interaction remains, or even strengthens, during the phase transition.

It has to be underlined that in all of the published halogenated structures, the presence of short intermolecular Hal···Hal contacts was observed. Hereafter, we will focus on these, comparing Cl···Cl to Br···Br interactions and halogen to hydrogen bonding.

The isostructural features observed in C_6Cl_6 and C_6Br_6 permit one to perform the crystal structure description of both compounds by analyzing one out of the couple. Thus, we will mostly focus on the description of the bromine-containing structure, and then we will discuss the main differences in the intermolecular distances with the chlorine-containing compound. We have redetermined the C_6Br_6 crystal structure at low temperature ($T = 100$ K) by using X-ray diffraction data. As for the previously reported room-temperature structure,[43] we also observed that C_6Br_6 crystallizes in the monoclinic system, space group $P2_1/n$ (see Table 1). One-half of the molecule belongs to the asymmetric unit, the second half being generated by an inversion center located in the middle of the molecular ring. In the crystal structure, C_6Br_6 molecules stack in columns along the *b*-axis direction. Molecules lying in alternated columns A and B (Figure 1a) exhibit an interplanar angle of 130.1°. The columns alternate in such a way that each type A column is surrounded by six other columns, two of type A and four of type B (see Figure 1b). This location allows for short Hal···Hal intercolumn interactions. Thus, six bromine atoms of a given molecule are involved in the bonding with ten closer bromines belonging to neighboring molecules by means of three center halogen

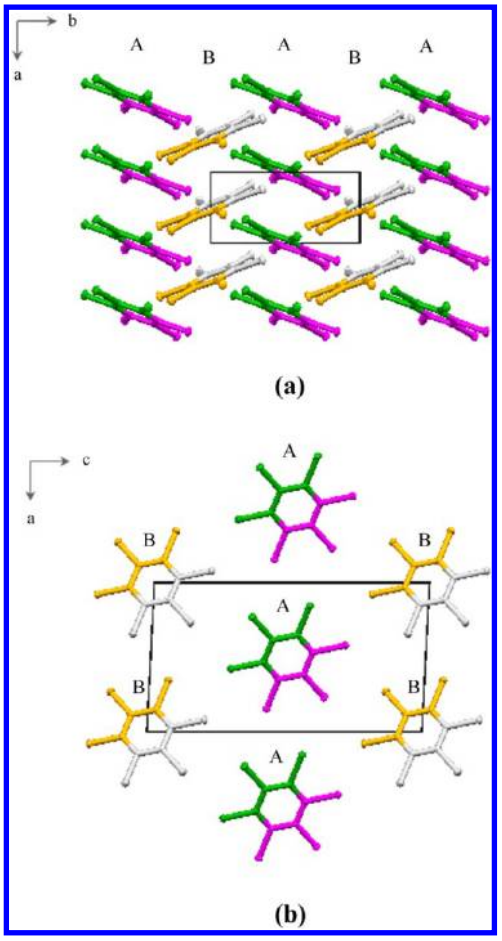

Figure 1. Crystal structure of C_6Br_6. (a) Side view of the alternating columns A and B projected in the *ab* plane. (b) Down view of the A and B columns projected in the *ac* plane. Colors of the molecules are defined by symmetry operations (excluding lattice translations): gray (x, y, z), orange ($-x, -y, -z$), green ($-x, 1/2 + y, 1/2 - z$), violet ($1/2 + x, 1/2 - y, 1/2 + z$).

synthon (Hal_3-synthon) formation and single Hal···Hal interactions (Figure 2a).

Along the *b*-axis direction the stacked molecules are close to each other with an interplanar distance of 3.583 Å and a slipping angle of 20.8°. Interatomic contacts of types C···C, Br···Br, and Br···C are also found between each two adjacent stacked molecules (Figure 2b), with the shortest Br···C distance of 3.654 Å. It should be noted that the later contact exhibits an interatomic distance that is close to the sum of the van der Waals radii of the Br and C_{sp2} atoms ($r_{vdw}(Br) + r_{vdw}(C_{sp2}) = 3.63$ Å).[48] From the mechanical properties observed in the isostructural C_6Cl_6 compound,[49] $\pi\cdots\pi$ interactions seem to provide the rigidity of the columns, increasing the contact between the molecules along the *b*-axis direction.

In the present study, it is observed that the crystal structure of C_6Br_5OH forms a molecular arrangement analogous to the one of C_6Br_6 (and of the isostructural C_6Cl_6), leading to similar molecular orientations and bonding networks (intra- and intermolecular interactions). However, the substitution of one bromine atom by a hydroxyl-group in C_6Br_5OH leads to the loss of the inversion centers, found in the crystal structure of C_6Br_6, lowering the space group symmetry. Though, C_6Br_5OH crystallizes in the monoclinic system ($P2_1$ space group) with one molecule in the asymmetric unit. As in C_6Br_6, the molecules stack

dx.doi.org/10.1021/cg300978x | *Cryst. Growth Des.* 2012, 12, 5373−5386

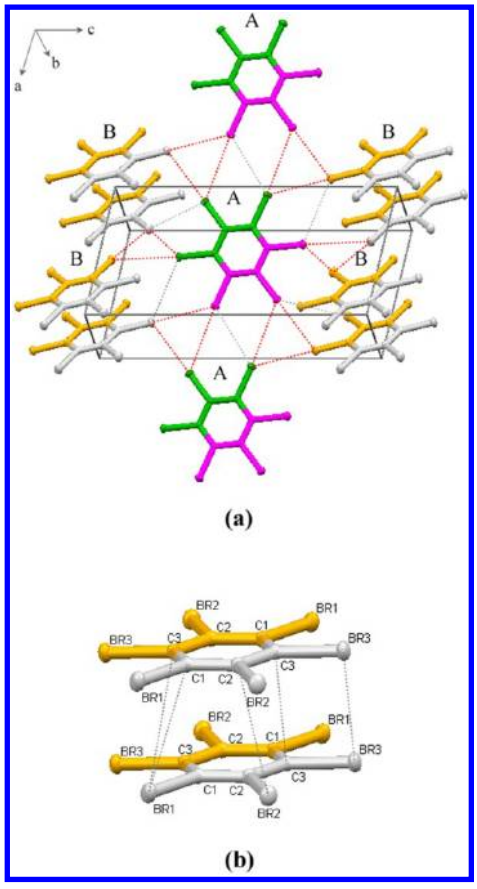

Figure 2. Intermolecular interactions in the crystal structure of C_6Br_6. (a) Intercolumn Hal_3-synthon interactions are noted in red dashed lines, while single Hal···Hal bonding is shown in gray. (b) Intracolumn interactions along the *b*-axis direction. Each Hal-atom makes two type-II interactions (within a synthon) and one of type-I with molecules in adjacent columns, while it makes two type-I contacts with adjacent molecules within the same column.

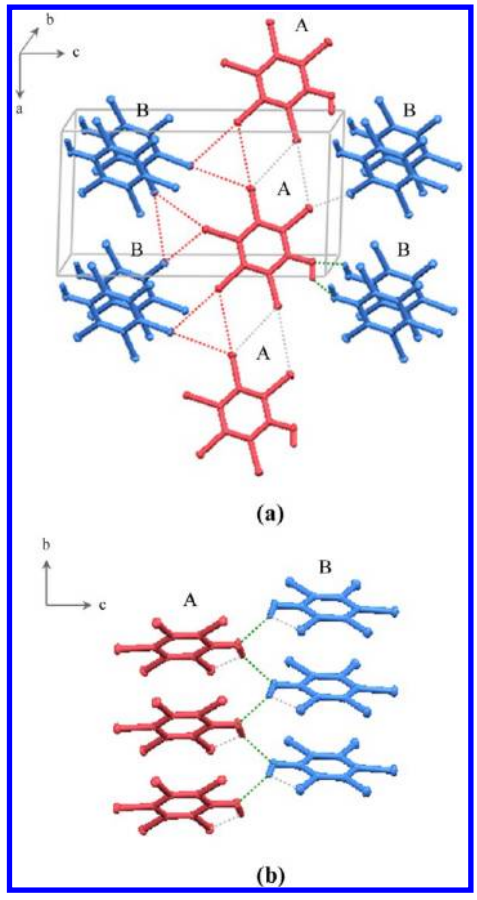

Figure 3. Interactions in the structure of C_6Br_5OH. (a) Hal_3-synthon interactions are noted in red, single halogen bonding in gray, and HB in green dashed lines. (b) HB network along the *b*-axis direction is noted in green, while intramolecular O−H···Br is shown in gray dashed lines. Colors of molecules are defined by symmetry operations (excluding lattice translation): red (x, y, z), blue $(-x, 1/2 + y, -z)$.

along the *b*-axis direction forming columns, the interplanar distance and the slipping angle being equal to 3.568 Å and 29.5°, respectively. The alternating columns A and B are assembled via hydrogen and halogen bonds (Figure 3). As observed for C_6Br_6, each column here is also surrounded by six neighboring ones. The synthon formation in the intercolumn region involves only three bromine atoms of each molecule, placed in *meta*- and *para*-positions with respect to the hydroxyl group, while bromines in *ortho*-positions form short single contacts with adjacent molecules (Figure 3a).

The presence of the OH-group leads to the hydrogen-bond formation (O−H···O) that links the molecules into infinite chains along the *b*-axis direction (Figure 3b), resembling several other mono and dihydric phenols.[50] While O···O and H···O distances are 2.849 and 2.23 Å, the O−H···O angle is found to be quite low (120.9°). From the crystal structure, the H-atom seems also to be involved in an intramolecular hydrogen bond with the adjacent *ortho*-Br atom, the H···Br distance being only 2.28 Å. As compared to the previously investigated phenol groups,[50] the bifurcation of the hydrogen bond can be a reason for a low intermolecular hydrogen-bond angle.

The C_6Br_5OH structure, determined at 100(4) K, turned out to be different from the known one reported by Betz et al. at 200(2) K.[47] In both cases, the crystal system is monoclinic, but the crystal structures differ in their space groups ($P2_1$ vs $C2/c$), number of molecules in the unit cell (2 vs 8), and number and length of halogen and hydrogen bonding. Thereby, using the sublimation method, we obtained the LT phase described by Wójcik et al.,[44] indicating that the crystallization method plays a conclusive role in phase determination even at low temperature.

Earlier studies showed that crystal structures with high *Z* values represent high energy minima in the crystallization pathway, therefore being less stable in comparison with the corresponding low-*Z* phases.[4a,51] On the basis of these findings, it can be suggested that the $C2/c$ phase ($Z = 8$), obtained by recrystallization from the boiling toluene, corresponds to a less stable and kinetically formed structure, while the $P2_1$ phase ($Z = 2$), obtained by sublimation method, is thermodynamically stable.

The structure of C_6Cl_5OH was also investigated. Similarly to the case described in the literature at room temperature by Sakurai,[45] C_6Cl_5OH displays the LT phase determined at 100(4) K (see Table 1). Figure 4 shows two different projections of the C_6Cl_5OH structure. The molecules form columns by stacking along the *b*-axis direction, the interplanar distance and the slipping angle being equal to 3.389 Å and 31.5°, respectively. Molecules lying in alternating columns A and B, C and D exhibit an interplanar angle of 91.8°.

As seen in Figure 5a, each column (e.g., column B) is surrounded by six other columns, similarly to the previously described structures. However, in the case of C_6Cl_5OH structure, the short contacts (synthons and single contacts) are formed

dx.doi.org/10.1021/cg300978x | *Cryst. Growth Des.* 2012, 12, 5373−5386

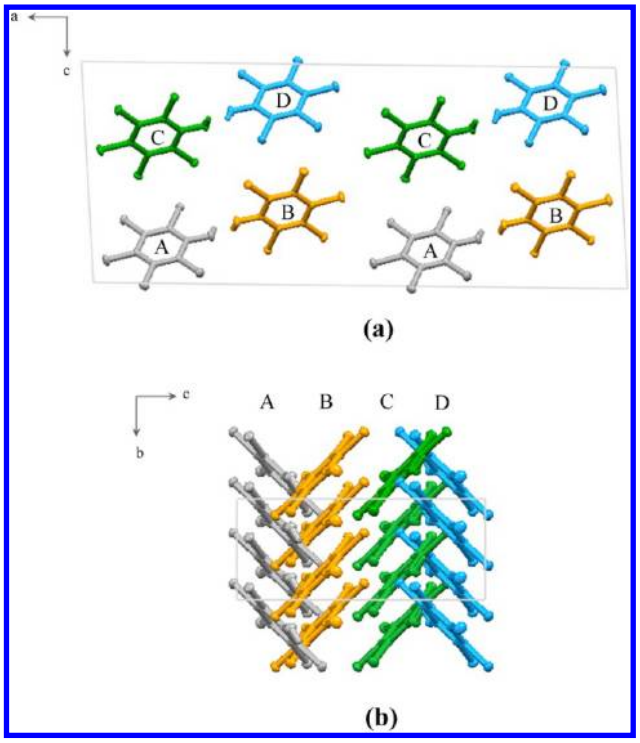

Figure 4. Crystal structure of C_6Cl_5OH. (a) Down view of the unit cell projected in the *ac* plane. (b) Side view of alternating columns projected in the *bc* plane. Colors of molecules are defined by symmetry operations (excluding lattice translation): blue (x, y, z), gray ($-x$, $-y$, $-z$), green ($-x$, y, $1/2 - z$), orange (x, $-y$, $1/2 + z$).

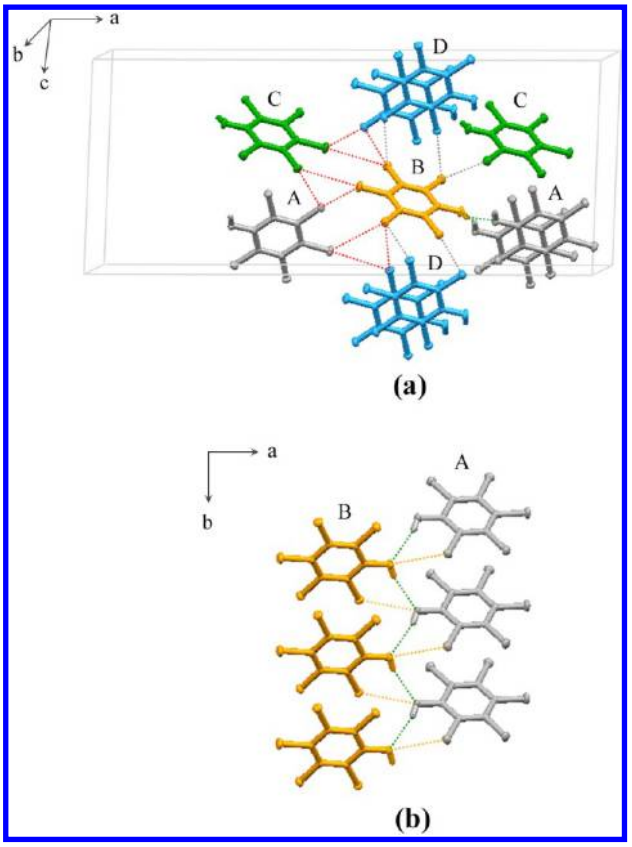

Figure 5. Intermolecular interactions in the structure of C_6Cl_5OH. (a) Hal_3-synthon interactions are noted in red, single halogen bonding in gray, and HB in green dashed lines; (b) HB network along the *b*-axis direction is noted in green, while intermolecular O···Cl contacts are shown as yellow dashed lines.

with nine instead of ten neighboring C_6Br_5OH molecules. The intermolecular hydrogen-bond pattern of C_6Br_5OH is also present in the C_6Cl_5OH structure (Figure 5b), with O···O and H···O distances of 2.928 and 2.04 Å, respectively, and a O−H···O angle of 151.7°. The former distance is longer than the one observed for C_6Br_5OH (2.849 Å). A short intermolecular contact between the oxygen and one of the halogen atoms in *ortho*-position is present in C_6Cl_5OH (O···Cl = 3.241 Å), forming a bifurcated interaction as previously reported.[45]

The C_6Cl_5OH crystal structure, which coincides with the one obtained by Sakurai,[45] does not show isostructural trends with C_6Br_5OH; however, it exhibits similar intermolecular halogen contacts that take place in C_6Br_5OH, as well as in C_6Cl_6 and C_6Br_6. All these contacts are discussed in the following part.

Structural Characterization of Hal_3-Synthons. We have shown that C_6Cl_6, C_6Br_6, and C_6Br_5OH ($P2_1$ phase) share a significant degree of halogen-bonding similarity. Halogen atoms in these structures form the so-called Hal_3-synthon, which is based on three center Hal···Hal interactions and behaves as a structure-assembling motif (Scheme 1d).

From the geometry of the Hal_3-synthon, the structural parameters characterizing the interaction are the intermolecular distances (d_i, i = 1, 2, 3) and the geometrical angles (θ_1 and θ_2), which are defined around each halogen atom. The Hal···Hal distances are compared to the corresponding sum of the van der Waals radii ($\sum r_{vdw}(Br) = 3.7$ Å, $\sum r_{vdw}(Cl) = 3.5$ Å) that are used to calculate the penetration of the van der Waals spheres ($\omega = d_i/\sum r_{vdw}(Hal)100\%$) in Table 2.

The Hal_3-synthons are cyclic and geometrically similar to $(OH)_3$ trimers, a common aggregation motif in the crystal structure of alcohols.[52] The C−Hal···Hal angles (θ_1 and θ_2) are similar in the C_6Br_6, C_6Br_5OH ($P2_1$ phase) and C_6Cl_6 crystal structures (Table 2). One interaction is almost linear (on average, $\theta_1 = 174.1 \pm 1.7°$), and the other is oblique (on average, $\theta_2 = 120.7 \pm 3.4°$). According to the geometrical features of these interactions, Hal_3-synthons could be classified as a particular case of type-II ($\theta_1 \approx 90°$, $\theta_2 \approx 180°$) Hal···Hal interactions. A special case concerns the three-center Hal_3-contact found in C_6Cl_5OH ($C2/c$ phase). Indeed, while three short Hal···Hal interactions seem to form a synthon (Figure 5a), two of its six structural contact angles (Table 2) deviated significantly from the expected ones in Hal_3-synthons ($\theta_1 \approx 120°$ and $\theta_2 \approx 180°$). However, as the interactions in all of the mentioned synthons are formed by facing electron deficient and electron concentration regions, the discussion in the following part concerns all of them in the four studied structures.

Electron Density Modeling and Analysis of Hal···Hal Interactions in Hal_3-Synthons from the Topology of the $\rho(\mathbf{r})$ Function. The deformation of the static electron density, $\Delta\rho(\mathbf{r})$, is defined as the difference between the multipolar and the spherical atom models (see the Supporting Information). For C_6Cl_6 and C_6Cl_5OH, the $\Delta\rho(\mathbf{r})$ map shows a deficiency of electron density (δ^+) with respect to the spherical noninteracting atoms in the regions along the C−Cl bonding axes, behind the halogen atom, and a charge density excess (δ^-) in the planes perpendicular to the bonds around chlorine nuclei[15] (Figure 6a,c).

The experimental model of C_6Cl_6 was recently compared to the one calculated against theoretical structure factors issued from periodic DFT calculations, showing a very good matching

dx.doi.org/10.1021/cg300978x | *Cryst. Growth Des.* 2012, 12, 5373−5386

Table 2. Halogen-Bonding Geometry of Hal_3-Synthons in C_6Cl_6, C_6Cl_5OH, C_6Br_6, and C_6Br_5OH[a]

	interaction	d (Å)	ω (%)	θ_1 (deg)	θ_2 (deg)
C_6Cl_6	$Cl_1^{i}\cdots Cl_2^{ii}$	3.4466(1)	98.4	116.73(2)	175.03(2)
	$Cl_2^{ii}\cdots Cl_3^{iii}$	3.4701(1)	99.1	124.17(2)	174.75(2)
	$Cl_3^{iii}\cdots Cl_1^{i}$	3.6662(1)	104.7	123.30(1)	171.20(2)
C_6Cl_5OH	$Cl_4^{i}\cdots Cl_2^{vi}$	3.4095(1)	97.4	*78.28(2)*	175.10(0)
	$Cl_2^{vi}\cdots Cl_3^{vii}$	3.6476(2)	104.2	126.45(1)	*110.26(2)*
	$Cl_3^{vii}\cdots Cl_4^{i}$	3.6197(2)	103.4	122.14(2)	177.55(2)
C_6Br_6	$Br_1^{i}\cdots Br_2^{ii}$	3.5412(2)	95.7	115.11(1)	174.18(1)
	$Br_2^{ii}\cdots Br_3^{iii}$	3.5551(4)	96.1	123.83(1)	176.68(1)
	$Br_3^{iii}\cdots Br_1^{i}$	3.7761(2)	102.1	122.77(1)	171.20(2)
C_6Br_5OH	$Br_2^{i}\cdots Br_3^{iv}$	3.5066(2)	94.8	117.33(1)	173.35(1)
	$Br_3^{iv}\cdots Br_4^{v}$	3.6576(2)	98.8	122.58(1)	173.04(1)
	$Br_4^{v}\cdots Br_2^{i}$	3.7127(3)	100.3	120.73(1)	175.72(1)

[a]Distances (d_i, i = 1, 2, 3) and angles ($\theta_1 < \theta_2$) are depicted in Scheme 1d. The ω parameter measures the penetration of the van der Waals spheres (ω < 100%) or their separation (ω > 100%). The structural parameters correspond to the multipolar model described in the following section. The particular Hal_3-geometry found in C_6Cl_5OH is depicted by one θ_1 and one θ_2 value in italics. Symmetry codes: (i) x, y, z; (ii) $3 - x, -y, -z$; (iii) $1/2 + x, 1/2 - y, -1/2 + z$; (iv) $2 - x, -1/2 + y, 1 - z$; (v) $1 + x, 1 + y, z$; (vi) $x, 3 - y, -1/2 + z$; (vii) $-x, 3 - y, -z$.

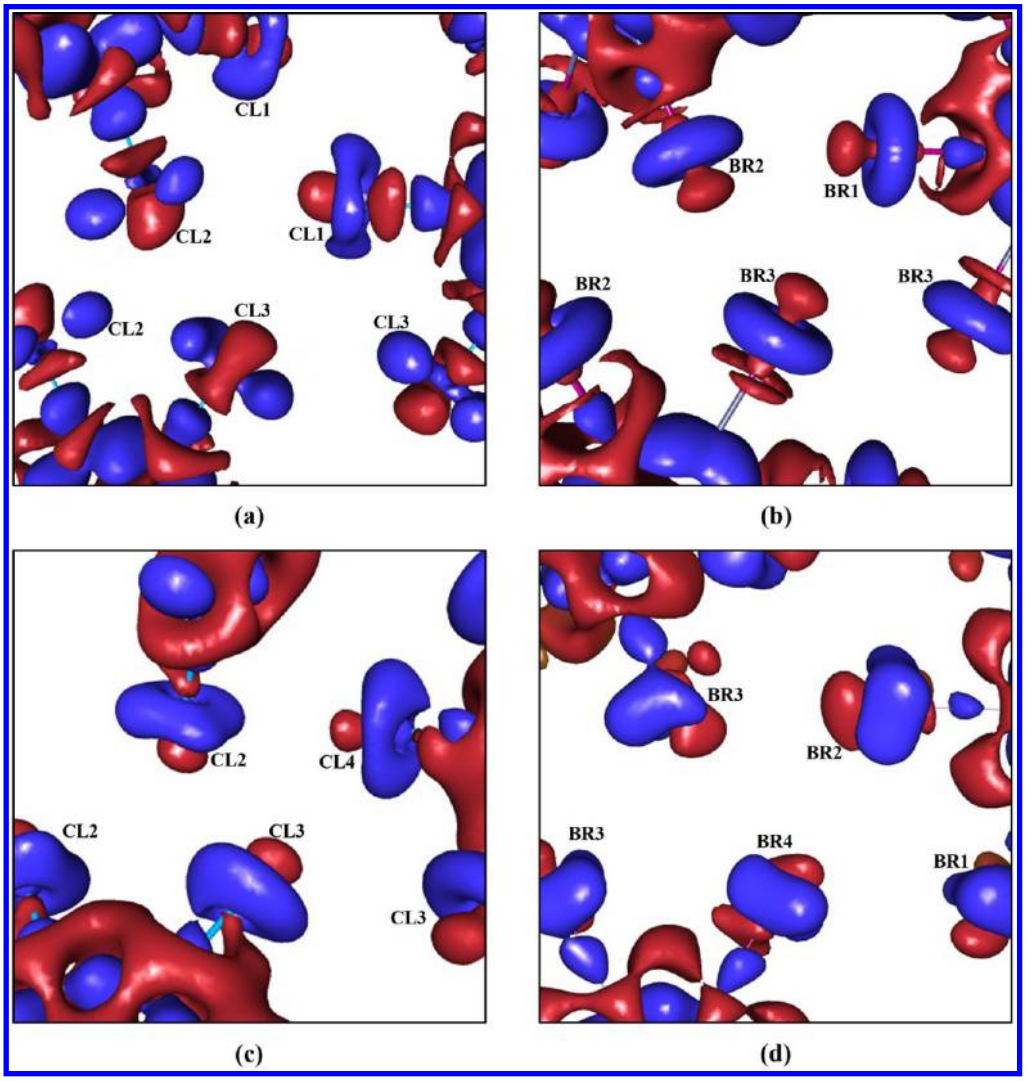

Figure 6. Static deformation density maps of the Hal_3-synthons in the structures of (a) C_6Cl_6, (b) C_6Br_6 (theoretical calculations), (c) C_6Cl_5OH, and (d) C_6Br_5OH. The iso-surfaces are drawn at 0.05 e Å^{-3}. Positive and negative values are represented in blue and red, respectively. For C_6Cl_6, the map corresponding to theoretical calculations can be found in ref 17.

between them for most of the derived electron properties.[17] The main differences were found in the more contracted theoretical density close to the halogen nuclei. Theoretical calculations exhibit a more symmetric deformation of the electron density around the chlorine nuclei, while keeping the same relative orientations of δ^- and δ^+ regions. The $\Delta\rho(\mathbf{r})$ map of C_6Br_6,

dx.doi.org/10.1021/cg300978x | *Cryst. Growth Des.* 2012, 12, 5373−5386

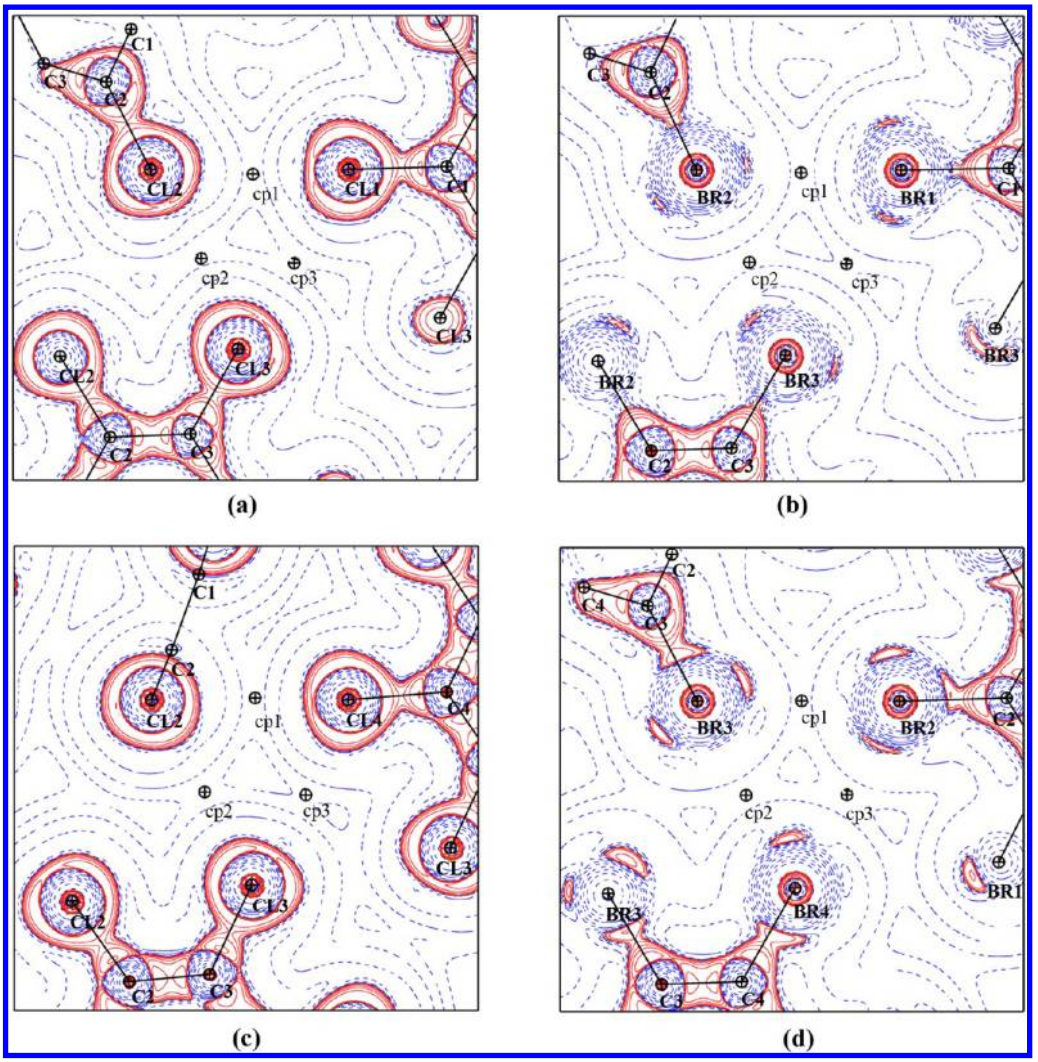

Figure 7. $L(\mathbf{r}) = -\nabla^2\rho(\mathbf{r})$ maps with the observed (3, −1) intermolecular bond critical points (cp) of $\rho(\mathbf{r})$ drawn in the plane of the Hal_3-synthon for (a) C_6Cl_6, (b) C_6Br_6 (theoretical calculations), (c) C_6Cl_5OH, and (d) C_6Br_5OH. Logarithmic contours in e Å^{-5}. Red and blue contours denote positive and negative values, respectively. For C_6Cl_6, the map corresponding to theoretical calculations can be found in ref 17.

obtained from the theoretical calculations, discloses features similar to those found in the experimental $\Delta\rho(\mathbf{r})$ maps of the C_6Br_5OH molecule, while both of them exhibit very alike torus-shaped regions of charge accumulation around bromine nuclei (Figure 6b,d), as previously observed for chlorines in C_6Cl_6 and C_6Cl_5OH. Thereby, both experimental and theoretical $\Delta\rho(\mathbf{r})$ maps provide a good description of the aspherical nature of charge density distribution around bromine and chlorine atoms, clearly bringing out the "polar flattening effect"[6] at the intermolecular Hal···Hal regions in all of the four compounds, the δ^- and δ^+ regions being situated in a similar way for all of them, as in those observed in chloranil.[33b] From Figure 6, the four $\Delta\rho(\mathbf{r})$ maps representing the Hal_3-synthons are qualitatively similar and specifically show that electron-excess and electron-deficient regions face each other along the three synthon edges, suggesting directional $\delta^-\cdots\delta^+$ interactions.

In Figure 7, the contour maps of the $L(\mathbf{r})$ function, which corresponds to the negative Laplacian of electron density $-\nabla^2\rho(\mathbf{r})$, are displayed for the four Hal_3-synthons, indicating the anisotropic nature of the charge distribution around halogen nuclei. For Cl atoms, the charge concentration (CC) and charge depletion (CD) sites are respectively located in δ^- and δ^+ regions and correspond to nucleophilic and electrophilic sites around the halogen nuclei, as previously shown in solid chlorine,[53] chlorinefluoride,[53b] and hexachlorobenzene.[15] From their relative positions within the four discussed synthons, CC and CD regions face each other along the three directions of this structural motif, indicating attractive electrophilic−nucleophilic (CD···CC) interactions.

To characterize the Hal···Hal interactions, we focus on the local properties of $\rho(\mathbf{r})$ at the bond CPs (see the Supporting Information for a detailed description) of the four given compounds obtained from both experimental and theoretical (the case of C_6Br_6) modeling. The properties are the electron density ρ, the curvatures of the electron density ($\lambda_1, \lambda_2 < 0, \lambda_3 > 0$) along the bonding direction (λ_3) and in the perpendicular plane (λ_1, λ_2), the Laplacian $\nabla^2\rho$ ($\nabla^2\rho = \lambda_1 + \lambda_2 + \lambda_3$) and the local electron kinetic G, potential V, and total H ($H = G + V$) energy densities. Because of the mixed effects of the different valence shells involved in their respective contacts, it is not straightforward to measure the difference in the interaction intensity between Br···Br and Cl···Cl from a direct comparison of their ρ, $\nabla^2\rho$, V, and G values only. However, one can approach the problem by using normalized quantities per charge density unit, such as the ratio $(|V|/\rho)/(G/\rho) = |V|/G$. This descriptor permits one to undertake a quantitative classification of pure

dx.doi.org/10.1021/cg300978x | Cryst. Growth Des. 2012, 12, 5373−5386

Table 3. Topological Characteristics for Each Pairwise Intermolecular Interaction Belonging to the Hal_3-Synthons in C_6Cl_6, C_6Cl_5OH, C_6Br_6, and C_6Br_5OH[a]

	interaction	d (Å)	ρ	$\nabla^2\rho$	λ_1	λ_2	λ_3	G	V	$\lvert V\rvert/G$	E_{int}	ΔL	$\Delta(L/\rho)$
C_6Cl_6[b]	$Cl_1^{i}\cdots Cl_2^{ii}$	3.4466(1)	0.049	0.62	−0.09	−0.08	0.79	13.3	−9.7	0.73	4.9	11.4	5.6
			0.045	*0.59*	*−0.10*	*−0.10*	*0.78*	*12.5*	*−8.9*	*0.71*	*4.5*	*11.7*	*5.2*
	$Cl_2^{ii}\cdots Cl_3^{iii}$	3.4701(1)	0.057	0.57	−0.15	−0.14	0.87	12.8	−10.4	0.82	5.2	10.3	4.5
			0.041	*0.56*	*−0.09*	*−0.09*	*0.74*	*11.7*	*−8.1*	*0.69*	*4.1*	*10.8*	*5.6*
	$Cl_3^{iii}\cdots Cl_1^{i}$	3.6662(1)	0.038	0.41	−0.09	−0.09	0.59	8.8	−6.4	0.73	3.2	9.7	3.8
			0.028	*0.38*	*−0.05*	*−0.05*	*0.48*	*7.7*	*−5.1*	*0.66*	*2.6*	*10.7*	*5.4*
C_6Cl_5OH	$Cl_4^{i}\cdots Cl_2^{vi}$	3.4095(1)	0.058	0.60	−0.13	−0.11	0.84	13.6	−10.9	0.80	5.5	12.5	5.3
	$Cl_2^{vi}\cdots Cl_3^{vii}$	3.6476(2)	0.039	0.47	−0.10	−0.09	0.66	10.0	−7.1	0.71	3.6	11.3	5.0
	$Cl_3^{vii}\cdots Cl_4^{i}$	3.6197(2)	0.039	0.41	−0.10	−0.08	0.59	8.8	−6.5	0.74	3.3	10.7	4.4
C_6Br_6[c]	$Br_1^{i}\cdots Br_2^{ii}$	3.5412(2)	0.066	0.62	−0.15	−0.15	0.92	14.7	−12.5	0.85	6.3	3.0	4.8
	$Br_2^{ii}\cdots Br_3^{iii}$	3.5551(4)	0.064	0.61	−0.14	−0.14	0.89	14.3	−12.0	0.84	6.0	2.9	4.8
	$Br_3^{iii}\cdots Br_1^{i}$	3.7761(2)	0.042	0.41	−0.09	−0.09	0.59	9.1	−6.9	0.76	3.5	2.8	4.6
C_6Br_5OH	$Br_2^{i}\cdots Br_3^{iv}$	3.5066(2)	0.063	0.66	−0.15	−0.12	0.93	14.8	−12.4	0.84	6.2	6.8	10.9
	$Br_3^{iv}\cdots Br_4^{v}$	3.6576(2)	0.051	0.53	−0.10	−0.10	0.73	11.7	−9.2	0.79	4.6	6.5	8.5
	$Br_4^{v}\cdots Br_2^{i}$	3.7127(3)	0.047	0.47	−0.09	−0.09	0.65	10.5	−8.1	0.77	4.1	5.2	6.9

[a]The parameters ρ (e Å^{-3}), $\nabla^2\rho$ (e Å^{-5}), $\lambda_{i,i=1,2,3}$ (e Å^{-5}), G, and V (kJ mol^{-1} bohr^{-3}) are calculated at the CPs of $\rho(\mathbf{r})$. ΔL (e Å^{-5}) and $\Delta(L/\rho)$ (Å^{-2}) parameters are calculated as the difference between the values observed at the CD and CC sites of the interacting atoms. E_{int} (kJ mol^{-1}) values are estimated as $-(1/2)V$, the constant being in bohr^3 units. See Table 2 for symmetry codes. [b]First and second lines correspond to experimental and theoretical (VASP calculations)[17] data. [c]Values are from theoretical (VASP calculations) data.

closed-shell ($|V|/G < 1$), pure shared-shell ($|V|/G > 2$), and intermediate interactions between these electronic states ($1 < |V|/G < 2$) in a common framework due to the normalization of the energetic quantities.[54]

According to the topological and energetic properties of $\rho(\mathbf{r})$ at CPs (Table 3), all of the mentioned Hal···Hal contacts exhibit typical features of pure closed-shell interactions: the values of ρ are relatively low ($0.038 < \rho < 0.058$ e Å^{-3} for Cl···Cl; $0.042 < \rho < 0.066$ e Å^{-3} for Br···Br), and those of $\nabla^2\rho$ are positive and low ($0.41 < \nabla^2\rho < 0.62$ e Å^{-5} for Cl···Cl; $0.41 < \nabla^2\rho < 0.66$ e Å^{-5} for Br···Br), both being typical of weak hydrogen bonds.[54] Furthermore, the magnitudes of the kinetic energy density are greater than those of the potential energy density, leading to $|V|/G < 1$ and $H > 0$, therefore illustrating that these mainly electrostatic ($\delta^+\cdots\delta^-$) interactions are very weak.[52,54]

The phenomenological correlation between the interaction energy and the potential energy density at CPs ($E_{int} \sim -(1/2)V^{CP}$)[55] was first proposed for hydrogen-bonded systems.[40a] This reported relationship has been also used as an estimation of the interaction energy in the experimental analysis of $\rho(\mathbf{r})$ when other types of pure closed-shell interactions are involved,[56] including halogen-bonded systems.[13,57] According to this estimation, E_{int} has been evaluated for each Hal···Hal interaction within a synthon (Table 3), the average value being of 4.3 ± 1.0 kJ mol^{-1} for Cl···Cl and of 5.1 ± 1.2 kJ mol^{-1} for Br···Br (rms deviations are given to report statistical dispersion in the values). It is noteworthy that, at similar distances, the estimated E_{int} values for Cl···Cl interactions are very close to those recently reported for Cl···Cl type-II (4.8 kJ mol^{-1}) intermolecular contacts.[13] Comparing the estimated E_{int} values for Cl···Cl and Br···Br interactions, the later was found to be 17% more intense than the former. This observed tendency is in accordance with crystallographic and theoretical studies of Awwadi et al.,[58] showing that the strength of these contacts decreases in the order I···I > Br···Br > Cl···Cl. The calculated $|V|/G$ magnitudes (Table 3) also follow a similar trend, being on average 0.76 ± 0.04 and 0.81 ± 0.04 for Cl···Cl and Br···Br and showing 6% difference between them.

Analysis of Hal···Hal Interactions from the Topology of the *L*(r) Function. *Qualitative Description of the Laplacian Distribution for Cl- and Br-Atoms.* To begin this discussion, we would like to note that experimental and both periodic and gas-phase analyses performed for the halogenated compounds show a complex $L(\mathbf{r})$ topology, exhibiting a large number of CPs around the halogen nuclei. For the purpose of the present work, we focus only on those containing the main information needed for the analysis of the intermolecular interactions building the synthons, which are associated with the charge concentration (CC) and charge depletion (CD) regions in the valence shell of halogen atoms.

Figure 8 shows a typical $L(\mathbf{r})$ distribution around Cl- and Br-atoms obtained on the isolated C_6Cl_6, C_6Br_6, and $BrCH_2N(CH_3)_2$ molecules from MP2 calculations. For chlorine, both CC and CD sites, which are respectively associated with (3, −3) and (3, +1) CPs of the $L(\mathbf{r})$ function, belong to the valence shell charge concentration (VSCC) region of the atom. As a consequence, positive values of $L(\mathbf{r})$ correspond to both of these regions (Figure 8a).

This is not the case for bromine, for which the VSCC region is much more reduced, representing a three-dimensional belt of negative Laplacian in the outer electron shell of the atom. Accordingly, only CC (3, −3) sites belong to the VSCC, while the CD site is found in a largely extended $L(\mathbf{r}) < 0$ region, expanding from very short distances from the Br nucleus (Figure 8b,c). This is due to the overlap of charge depleted regions belonging to the outer electron shell and the closest inward one, which is characterized by a saddle point (i.e., a (3, −1) CP marked in red in Figure 8b,c) for the $L(\mathbf{r})$ function. In the crystal structures, the L magnitudes observed at these (3, −1) CPs are negatively pronounced and very close to each other ($-1836.9 < L < -1831.8$ e Å^{-5}, for Br-atoms in C_6Br_6 and C_6Br_5OH). In all cases, the (3, −1) CP is placed at 0.35 Å from the bromine nucleus. These extremely similar features observed for all of the bromine atoms analyzed in this work confirm that most of $\rho(\mathbf{r})$ around this (3, −1) CP belongs to a core electron shell that, in the multipolar modeling, is similarly defined for all of them and considered to remain unperturbed. As a consequence, the topological characteristics at the (3, −1) site cannot be used to compare the particular electrophilic power of the CD region of bromines within different environments.

dx.doi.org/10.1021/cg300978x | Cryst. Growth Des. 2012, 12, 5373−5386

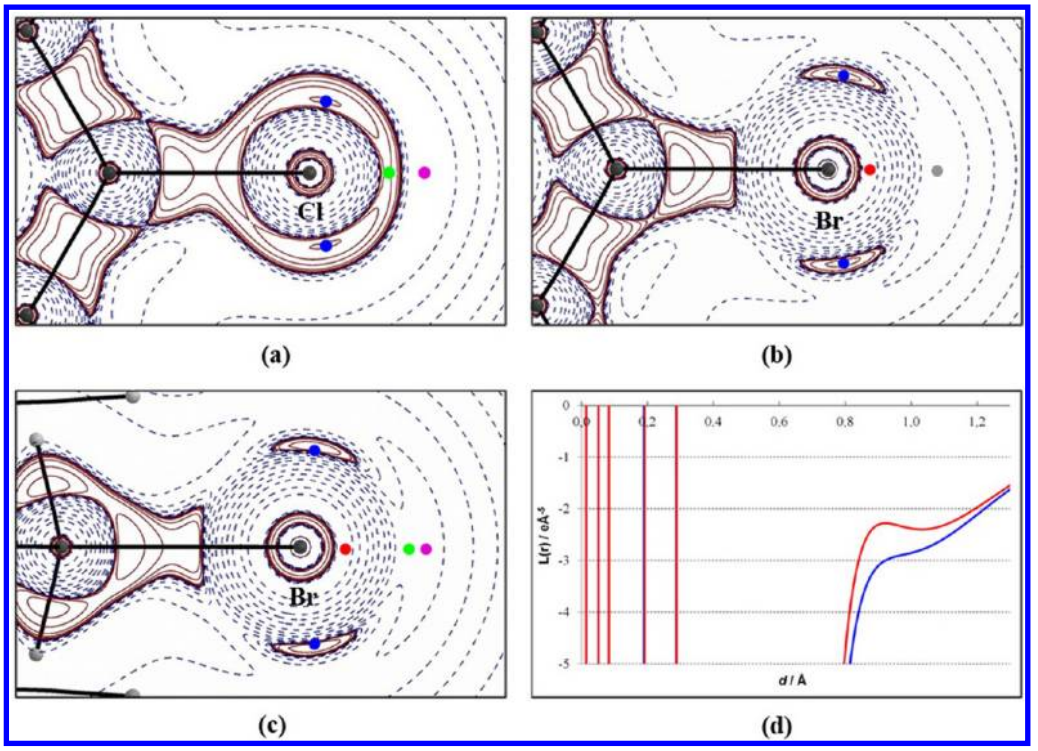

Figure 8. Contour maps of $L(\mathbf{r})$ around a Cl-atom in (a) C_6Cl_6 and around Br-atoms in (b) C_6Br_6 and (c) $BrCH_2N(CH_3)_2$ obtained from MP2 calculations in gas-phase. Red and blue contours denote positive and negative values of $L(\mathbf{r})$, respectively. In the outer electron shell, CC sites are characterized by local maxima of $L(\mathbf{r})$ ((3, −3) CPs marked in blue); the CD sites along the C−Hal bonding axis direction are characterized by either a couple of (3,+1) and (3, +3) CPs (respectively marked in grey and pink; case of a and c) or a plateau (characteristic site marked in gray; case of b). The minimum along the bonding axis direction ((3, −1) CP) of the closest inward shell is in red. (d) Plots of $L(\mathbf{r})$ along the C−Br bonding direction for C_6Br_6 (blue curve) and for $BrCH_2N(CH_3)_2$ (red curve). The positions of the bromine inner electron shells match in both compounds, whereas in the outer region the existence of (3,+1) and (3, +3) CPs in the case of $BrCH_2N(CH_3)_2$, and their absence in the case of C_6Br_6, is observed.

As compared to chlorine atoms, the important development of a very extended and significantly depleted electron density region in bromines is straightforwardly associated with the increasing character of the so-called σ-hole, first pointed out for heavier halogens.[59] Indeed, this highly specific electron distribution is the primary origin of the well-known electrophilic region along the C−Hal bonding axis direction (Figure 8), which increases from lighter to heavier halogens and is chemically represented by the increase of both the σ-hole and its concomitant positive electrostatic potential ($\varphi_{CD} > 0$). Accordingly, the more depleted is $\rho(\mathbf{r})$ in that region, the more important are the σ-hole and the magnitude of $\varphi_{CD} > 0$.

Depending on the activation of the bromine atom by the neighboring chemical groups, its outer electron shell at the CD site is characterized by the presence of either a couple of successive (3,+1) and (3,+3) CPs or by a plateau, namely an area where the variation of $L(\mathbf{r})$ is locally the smallest but its gradient does not vanish. For example, Figure 8c and d displays the $L(\mathbf{r})$ function in the case of the $BrCH_2N(CH_3)_2$ molecule: in this particular compound, the bromine atom is negatively charged due to the presence of the $-N(CH_3)_2$ electron-donating group ($q_{Br} = -0.27e$), and the two CPs associated with the CD site exist. In the case of C_6Br_6 (Figure 8b and d), where the bromine atom is slightly positively charged ($q_{Br} = +0.03e$), these two CPs are coalesced, resulting in an area of soft variation of $L(\mathbf{r})$ without the presence of a true CP. The location of the characteristic CD site in the plateau is determined by means of the derivative of the $L(\mathbf{r})$ function (see Figure S4 in the Supporting Information).

Characterizing CC and CD Sites from L Magnitudes: The Failure of Cl···Cl versus Br···Br Comparison. The L magnitudes at CC and CD sites in the outer electron shell can be used for a quantitative evaluation of these regions in the interaction of Cl- and Br-atoms with the environment. The observed CC and CD values for Cl-atoms in C_6Cl_6 and C_6Cl_5OH are $17.7 < L_{CC} < 19.9$ e Å^{-5} and $6.1 < L_{CD} < 9.0$ e Å^{-5}, respectively, while for Br-atoms in C_6Br_6 and C_6Br_5OH they are $0.5 < L_{CC} < 5.1$ e Å^{-5} and $-3.7 < L_{CD} < -2.3$ e Å^{-5}. Thus, $L_{CC} > 0$ decreases from Cl- to Br-atoms, whereas L_{CD} varies from positive to negative values, respectively. As previously explained, the nucleophilic power of the CC region increases with the positive value of L_{CC}, while the electrophilic one of the CD region parallels the decrease of L_{CD} from positive to negative values. As a result, the greater the difference $\Delta L = L_{CC} - L_{CD}$ in the face-to-face CC···CD regions, the more important is the electrophilic−nucleophilic Hal···Hal interaction. However, comparing Br···Br to Cl···Cl interactions, it follows that ΔL values in the former are systematically lower than in the latter (Table 3), in contrast with the expected result, which assumes Br···Br being more intense than Cl···Cl interactions. To explain this unexpected feature, it can be invoked the different electron shells involved in the outer electron distribution of Br- and Cl-atoms, leading to a more important screening of the outer electrons in bromines that significantly deplete their charge distribution. As a consequence, bromines reduce their VSCC region with respect to chlorines, inducing the concomitant decrease of L_{CC} magnitudes and therefore $L_{CC}(Br) < L_{CC}(Cl)$. The increased screening also depletes the electron distribution in the CD region of the bromines outer shell, leading to negative $L_{CD}(Br)$ values, in contrast to the positive ones observed for chlorines. As a result of the balance between CC and CD contributions, $\Delta L(Cl\cdots Cl)$ values are greater than

dx.doi.org/10.1021/cg300978x | *Cryst. Growth Des.* 2012, 12, 5373−5386

Table 4. Topological Characteristics of the Hal_3-Synthon in Each of the Four Compounds, along with the Corresponding Magnitudes of Other Inter- and Intramolecular HBs in C_6Cl_5OH and C_6Br_5OH (Figure 9)[a]

halogen bonding							
synthon	ρ_Σ	$\nabla^2\rho_\Sigma$	G_Σ	V_Σ	$\langle\lvert V\rvert/G\rangle$	$E_{int,\Sigma}$	$\Delta(L/\rho)_\Sigma$
C_6Cl_6[b]	0.144	1.60	34.9	−26.5	0.76	13.3	13.9
	0.143	*1.59*	*34.7*	*−26.3*	*0.76*	*13.2*	*16.2*
C_6Cl_5OH	0.136	1.48	32.4	−24.5	0.76	12.3	14.6
C_6Br_6[c]	0.172	1.64	38.1	−31.4	0.82	15.7	14.2
C_6Br_5OH	0.161	1.66	37.0	−29.7	0.80	14.9	26.3
hydrogen bonding							
interaction	ρ	$\nabla^2\rho$	G	V	$\lvert V\rvert/G$	E_{int}	$\Delta(L/\rho)$
$C_6Cl_5OH_{O-H\cdots O}$	0.092	2.07	43.5	−30.5	0.70	15.3	29.9
$C_6Br_5OH_{O-H\cdots O}$	0.105	1.63	37.0	−29.5	0.80	14.8	32.0
$C_6Br_5OH_{O-H\cdots Br}$	0.134	2.08	48.8	−40.9	0.84	20.5	13.8

[a]The parameters ρ_Σ (e Å^{-3}), $\nabla^2\rho_\Sigma$ (e Å^{-5}), G_Σ, V_Σ (kJ mol^{-1} bohr^{-3}), $E_{int,\Sigma}$ (kJ mol^{-1}), and $\Delta(L/\rho)_\Sigma$ (Å^{-2}) are calculated as the sum over the three pairwise interactions building the synthon, while $\langle\lvert V\rvert/G\rangle$ is taken as an average of the three corresponding parameters at CP. [b]First and second lines correspond to experimental and theoretical (VASP calculations)[17] data. [c]Values are from theoretical data.

ΔL(Br···Br), indicating that the ΔL parameter does not permit a straightforward comparison of the intermolecular interaction between different halogens.

The L/ρ Descriptor: Evaluating the Electrophilic–Nucleophilic Interaction from Δ(L/ρ). To overcome the problem, we introduce the normalized magnitude L/ρ (Å^{-2}), which measures the charge concentration ($L/\rho > 0$) or the charge depletion ($L/\rho < 0$) per charge density unit at the CC and CD sites located from the topology of $L(\mathbf{r})$ (see Table S6 in the Supporting Information).

Actually, the calculated difference $\Delta(L/\rho) = (L/\rho)_{CD} - (L/\rho)_{CC}$ for the three experimentally determined structures C_6Cl_6, C_6Cl_5OH, and C_6Br_5OH indicates the expected increase in intensity from Cl···Cl to Br···Br type-II interactions (Table 3). In contrast, results coming from C_6Br_6 theoretical calculations show some differences. Indeed, while improving their ranking from ΔL to $\Delta(L/\rho)$ classifications, they do not reach values similar to those in C_6Br_5OH, as expected from the comparison between C_6Cl_6 and C_6Cl_5OH, where $\Delta(L/\rho)$ values are very close to each other ($\langle\Delta(L/\rho)\rangle = 4.7 \pm 0.6$ Å^{-2}).

To reveal the origin of the observed difference between bromines in the experimental and theoretical crystal phases, theoretical calculations of the isolated molecules C_6Br_6 and C_6Br_5OH were performed (see Figure S5 and Tables S7, S8 in the Supporting Information). According to these calculations, the topological properties at CC and CD sites are extremely similar in both molecules, $\Delta(L/\rho)$ being 6.85 Å^{-2} for C_6Br_6 and on average 6.72 ± 0.02 Å^{-2} for C_6Br_5OH. With respect to gas-phase calculations, the topological values obtained for the corresponding crystal phases show lower magnitudes in the case of C_6Br_6 periodic theoretical calculations ($\langle\Delta(L/\rho)\rangle = 4.74 \pm 0.11$ Å^{-2}) and greater magnitudes for the experimental C_6Br_5OH structure ($\langle\Delta(L/\rho)\rangle = 8.77 \pm 2.00$ Å^{-2}). Thus, the case of C_6Br_6 repeats the same trend observed in the comparison of the gas and crystal phases of the Cl-containing compounds, for which the $\langle\Delta(L/\rho)\rangle$ values are 6.87 and 4.62 ± 0.88 Å^{-2} (C_6Cl_6), and 6.68 ± 0.02 and 4.87 ± 0.44 Å^{-2} (C_6Cl_5OH), for theoretical gas-phase and experimental models, respectively (see Table 3 and Table S8 in the Supporting Information). Moreover, gas-phase calculations earlier performed by different authors on other brominated molecules[60] also present more pronounced CC regions around Br-nuclei than in the case of the theoretical crystal phase of C_6Br_6. On the other hand, experimental and theoretical multipolar models in crystal phase are expected to give similar results, as observed in the comparison of the $\langle\Delta(L/\rho)\rangle$ values coming from the experimental and periodic theoretical data of C_6Cl_6,[17] which are found similar (4.62 ± 0.88 and 5.40 ± 0.22 Å^{-2}, respectively) even if the theoretical model exhibits slightly larger magnitudes. Overall, despite the high $\langle\Delta(L/\rho)\rangle_{C6Br5OH}$ value, which shows a high statistical dispersion, $\langle\Delta(L/\rho)\rangle$ decreases in most cases from gas to crystal phases. In addition to the intrinsic differences between the models used in gas and crystal phases (LCAO and multipolar) and to the effect of the basis used in the calculations, the pointed decrease of $\langle\Delta(L/\rho)\rangle$ could be also brought closer to the screening of the electrophilic–nucleophilic interactions induced by the dielectric constant of the crystal environment.

In summary, comparing Br- to Cl-atoms, $(L/\rho)_{CD}$ in the former exhibits a significant decrease from positive to negative values that overcomes the decrease of its positive $(L/\rho)_{CC}$ values, leading to a $\Delta(L/\rho)$ magnitude, and therefore to an electrostatic interaction, which is in general greater (in some cases is found comparable) than that found for chlorine atoms in type-II Hal···Hal interactions (see Table 3).

Analysis of Cl_3- and Br_3-Synthons from Topological and Energetic Criteria. Considering the Hal_3-motif as a structure-determining unit, we characterize it as the addition of three Hal···Hal contributions. Thus, according to the topological properties calculated at the CPs of the $\rho(\mathbf{r})$ function, all of the resulting magnitudes ρ_Σ, $\nabla^2\rho_\Sigma$, G_Σ, V_Σ and the average $\langle\lvert V\rvert/G\rangle$ increase from Cl_3- to Br_3-synthons (Table 4), indicating that Hal_3-motifs built with bromine atoms are stronger than those with chlorines. In addition to each Hal···Hal contact, the Hal_3-synthon can be also considered as a pure closed-shell interaction ($\langle\lvert V\rvert/G\rangle < 1$, see Table 4). Therefore, the interaction energy of the structure-determining unit ($E_{int,\Sigma}$) has been calculated from the estimation $E_{int,\Sigma} \sim -(1/2)\sum V^{CP}$, paralleling the empirical expression used for interactions of pure closed-shell type.[13,56,57] It should be noted that even if $E_{int,\Sigma}$ is an approximation to E_{int} of the trimer, because other interactions that involve the latter and are external to the synthon can contribute to E_{int}, $\rho(\mathbf{r})$ within the synthon reflects the influence of its environment. Accordingly, the $\rho(\mathbf{r})$ properties used to derive $E_{int,\Sigma}$ follow this effect, bringing closer the Hal_3-synthon contribution to E_{int} than the additional of three independent Hal···Hal interactions at the distances found in trimer. Thereby, the interaction energy $E_{int,\Sigma}$ of Cl_3-synthons is

dx.doi.org/10.1021/cg300978x | Cryst. Growth Des. 2012, 12, 5373−5386

on average 17% lower than that of Br_3-synthons. Moreover, comparing C_6Cl_6 to C_6Cl_5OH, and C_6Br_6 to C_6Br_5OH, the crystal structures not involving HB interactions exhibit Hal_3-synthons that are 8% and 5% stronger than those involving hydrogen bonds.

On the basis of the last considerations and the definition of the L/ρ descriptor, the $\Delta(L/\rho)_\Sigma$ parameter measures the electrophilic−nucleophilic interaction that takes part in the Hal_3-synthon, being mainly assumed electrostatic. Accordingly, this measure is on average ∼30% larger in Br_3-synthons (C_6Br_6 and C_6Br_5OH) than in Cl_3-synthons (C_6Cl_6 and C_6Cl_5OH).

Analysis of HB Interactions from the Topology of $\rho(\mathbf{r})$ and $L(\mathbf{r})$ Functions in C_6Cl_5OH and C_6Br_5OH. The particular feature of the structures containing the OH-group (C_6Cl_5OH and C_6Br_5OH) is the existence of HBs linking the molecules into an infinite chain along the *b*-axis direction at the opposite side of the molecule where halogens form Hal_3-synthons (Figures 3 and 5). As a consequence, HBs play a significant role in directing the packing of the molecules in the crystal lattice.

A first assumption about the existence and the significance of the HB in the present crystal structures was based on IR spectra.[44] Actually, the charge density approach and the associated topological analysis at the HB critical points (3, −1) allow us to evaluate quantitatively the strength of the interactions and to put it in comparison with that of Hal_3-synthons.

The topological parameters for the intermolecular and intramolecular HBs are given in Table 4 and correspond to the interactions shown in Figure 9. All of them are characterized as pure closed-shell interactions ($|V|/G < 1$). According to the previous studies,[54] the intermolecular O−H···O HBs in C_6Cl_5OH and C_6Br_5OH can be classified within those of weak strength ($5 < |E_{HB}| < 15$ kJ mol^{-1}). On the other hand, the intramolecular O−H···Br interaction exhibits a greater strength than the intermolecular HBs, its interaction energy being estimated from the value of the potential energy density at CP at $|E_{HB}| \sim 20$ kJ mol^{-1}.

Thus, the characterized energies that indicate weak intermolecular HB interactions in C_6Cl_5OH and C_6Br_5OH, and a stronger intramolecular HB in C_6Br_5OH, parallel the IR features observed in both C_6Cl_5OH and C_6Br_5OH structures, indicating a LT to HT phase transition associated with the breaking of intermolecular HBs and the remaining intramolecular HB in C_6Br_5OH of the HT phase.[44]

Comparison between Hal_3-Synthons and HB Interactions. From the estimated interaction energies, the intermolecular HB in C_6Cl_5OH is more energetic than the Cl_3-synthon by ∼3 kJ mol^{-1}, while in C_6Br_5OH this HB is mostly equivalent to the Br_3-synthon. This small comparative difference between C_6Cl_5OH and C_6Br_5OH crystal structures is mainly due to the small increase in $E_{int,\Sigma}$ of the Br_3-synthon with respect to that of the Cl_3-synthon, while E_{int} for the intermolecular HB remains almost unchanged from C_6Cl_5OH to C_6Br_5OH despite a less favorable orientation between the H- and O-atoms in C_6Br_5OH, as observed by both δ^-/δ^+ and CC/CD regions in $\Delta\rho$ and $\nabla^2\rho$ maps, respectively (Figure 9).

Comparing the electrostatic interaction in HBs and in synthons, as monitored from $\Delta(L/\rho)_\Sigma$, we observe that, whereas in C_6Br_5OH the magnitude is 20% larger in HB than in the synthon, in C_6Cl_5OH the difference rises to 50%. The differences fall, respectively, to ∼0% and 20% when considering the estimation of the total interaction energy. Overall, it indicates that the electrostatic contribution to the total interaction is greater in HBs than in Hal_3-synthons, and that the observed differences between them reduce in the total interaction energy due to other energetic

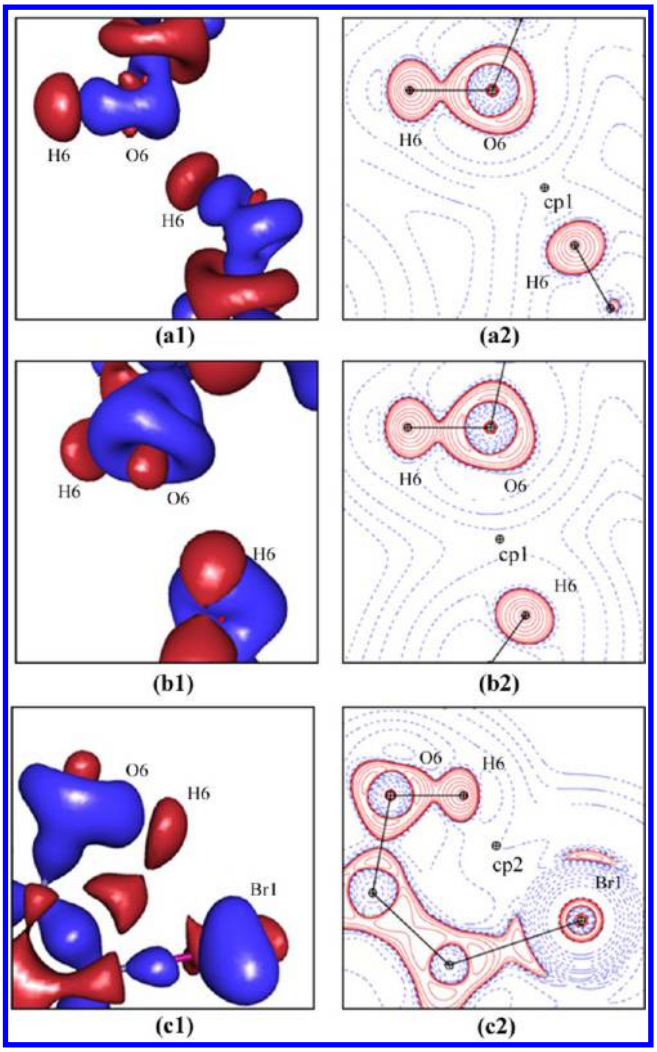

Figure 9. Static deformation density and $L(\mathbf{r})$ maps showing the intermolecular $H_6{-}O_6{\cdots}H_6$ interaction for C_6Cl_5OH (a1 and a2) and C_6Br_5OH (b1 and b2) and the intramolecular $O_6{-}H_6{\cdots}Br_1$ interaction for C_6Br_5OH (c1 and c2). The corresponding (3, −1) CPs are marked as cp1 and cp2, respectively. $\Delta\rho(\mathbf{r})$ iso-surfaces are drawn at 0.05 e Å^{-3}; positive values are in blue, negative are in red. $\nabla^2\rho(\mathbf{r})$ contours (e Å^{-5}) are in logarithmic scale; red and blue contours denote positive and negative values, respectively.

contributions, probably linked to the significant dispersion effects characterizing Hal···Hal interactions. A similar trend has been detected with the PIXEL energy decomposition[61] of C−H···X (X = N, O) and Br···Br interactions observed in the crystal structure of a polyhalogenated bipyridine compound,[62] where the dispersion contribution to the stabilization energy was found predominant for Hal···Hal. In contrast, it did not exhibit in the observed HBs. Furthermore, as in the present work, the electrostatic contribution (Coulombic plus polarization components) in HBs was shown larger than in Hal···Hal interactions.

CONCLUSION

The comparative study of trimers based on intermolecular halogen-bonding interactions (Cl_3- and Br_3-synthons) in terms of experimental and theoretical charge density analysis, followed by careful topological evaluation of properties, was performed. $\Delta\rho(\mathbf{r})$ and $L(\mathbf{r}) = -\nabla^2\rho(\mathbf{r})$ functions have revealed the anisotropic nature of charge distribution around the halogen

dx.doi.org/10.1021/cg300978x | Cryst. Growth Des. 2012, 12, 5373−5386

atoms giving rise to local charge concentration (CC or δ^-) and charge depletion (CD or δ^+) regions, which correspond to nucleophilic and electrophilic sites around the halogen nuclei. CC and CD face each other along the three directions within the four discussed synthons, indicating attractive electrophilic−nucleophilic interactions. According to the topological and energetic properties at bond critical points, all of the mentioned Hal···Hal contacts exhibit the character of pure closed-shell interactions. Synthons were analyzed as a unique structural motif, being characterized by the topological and energetic properties resulting from the addition of the contributions at the three bond critical points. In particular, the interaction energy of the Hal_3-synthons has been experimentally estimated as $E_{int,\Sigma} \sim -(1/2)\sum V^{CP}$, following the case of other pure closed-shell interactions. $E_{int,\Sigma}$, which is assumed to be close to the interaction energy of the trimer, is on average 17% larger in Br_3- than in Cl_3-synthons (∼15 and 13 kJ mol^{-1}, respectively), while single Cl···Cl and Br···Br interactions are very weak (∼4 and 5 kJ mol^{-1}, respectively).

Our study brings out, for the first time, the main difference between Cl_3- and Br_3-synthons, based on the topological analysis of the function $L(\mathbf{r}) = -\nabla^2\rho(\mathbf{r})$ and on the L/ρ descriptor. The intensity of the electrostatic interactions, measured from the electrophilic and nucleophilic power of the involved CD and CC regions, has been quantified by the difference in the Laplacian values normalized to charge density unit ($\Delta(L/\rho)$) at the topological critical points of the function $L(\mathbf{r})$ in these regions. The $\Delta(L/\rho)$ magnitudes in Cl_3- and Br_3-synthons parallel the calculated $E_{int,\Sigma}$ values, supporting our suggestion about a stronger interaction in the case of Br_3-synthons not only from the interaction energy point of view but also from the electrostatic interaction between the CC and CD regions.

Special attention has been also paid to the comparison of the Hal_3-synthons and HB interactions. The estimated $E_{int,\Sigma}$ values of Cl_3- and Br_3-synthons show magnitudes similar to those of HBs of small-medium strength. The comparison of Hal_3-synthons to intermolecular HBs in the crystal structures of C_6Cl_5OH and C_6Br_5OH indicates that, while their interaction energies are mostly equivalent in C_6Br_5OH, in C_6Cl_5OH E_{int} of HB is ∼20% larger than $E_{int,\Sigma}$ of Cl_3-synthon. Comparing the corresponding $\Delta(L/\rho)$ magnitudes, HBs exhibit electrostatic interactions ∼20% and 50% more intense than Br_3- and Cl_3-synthons. Accordingly, the electrostatic contribution increases from chlorine- to bromine-based synthons. On the other hand, a further contribution adds to the electrostatic one in the total interaction energy to bring closer the interaction energy of the Hal_3-synthon to that of HB. Most probably, this contribution is coming from dispersion effects that have not been analyzed in this work.

In summary, even though it is considered that halogen-bonding interactions play a secondary role with respect to the more dominant HB capabilities, the present results show that, when forming Hal_3-synthons, they could be as effective as HBs for supramolecular chemistry and crystal engineering purposes. Indeed, Hal_3-synthons are structurally recovered motifs in crystal environments due to a very important directional electrostatic recognition between δ^+/CD and δ^-/CC regions, thanks to their very well adopted dispositions in triangular motifs.

■ ASSOCIATED CONTENT

Supporting Information

Additional information on experimental details, theoretical methods, multipolar parameters, residual electron density maps, additional parameters at CC/CD sites of $L(r)$, results from the theoretical calculations of the isolated molecules C_6Cl_6, C_6Cl_5OH, C_6Br_6, and C_6Br_5OH, and crystallographic information files (CIF) for C_6Cl_5OH, C_6Br_5OH, and C_6Br_6 after multipolar refinement. This material is available free of charge via the Internet at http://pubs.acs.org.

■ AUTHOR INFORMATION

Corresponding Author

*E-mail: enrique.espinosa@crm2.uhp-nancy.fr.

Notes

The authors declare no competing financial interest.

■ ACKNOWLEDGMENTS

This work has been supported by the French "Agence Nationale de la Recherche" (Grant ANR-08-BLAN-0091-01). M.E.B. thanks the French ANR for a Ph.D. fellowship from the same grant. The "Service Commun de Diffraction X" of Université de Lorraine is thanked for providing access to crystallographic facilities. GENCI-CINES (Grant 2012-X2012085106) is thanked for providing access to computing facilities. We thank Dr. B. Guillot for his support and helpful discussions concerning the use of the MoPro program.

■ REFERENCES

(1) (a) Hassel, O.; Romming, C. *Q. Rev. (London)* **1962**, *16*, 1−18. (b) Hassel, O. *Science* **1970**, *170*, 497−502.

(2) Metrangolo, P.; Resnati, G. *Halogen Bonding: Fundamentals and Applications*; Springer: Berlin, 2008.

(3) Metrangolo, P.; Neukirch, H.; Pilati, T.; Resnati, G. *Acc. Chem. Res.* **2005**, *38*, 386−395.

(4) (a) Metrangolo, P.; Resnati, G. *Chem.-Eur. J.* **2001**, *7*, 2511−2519. (b) Corradi, E.; Meille, S. V.; Messina, M. T.; Metrangolo, P.; Resnati, G. *Angew. Chem., Int. Ed.* **2000**, *39*, 1782−1786.

(5) Clark, T.; Hennemann, M.; Murray, J. S.; Politzer, P. *J. Mol. Model.* **2007**, *13*, 291−296.

(6) Desiraju, G. R. *Crystal Engineering: The Design of Organic Solids*; Elsevier: Amsterdam, 1989.

(7) (a) Sakurai, T.; Sundaralingam, M.; Jeffrey, G. A. *Acta Crystallogr.* **1963**, *16*, 354−363. (b) Ramasubbu, N.; Parthasarathy, R.; Murray-Rust, P. *J. Am. Chem. Soc.* **1986**, *108*, 4308−4314. (c) Desiraju, G. R.; Pathasarathy, R. *J. Am. Chem. Soc.* **1989**, *111*, 8725−8726.

(8) Pedireddi, V. R.; Reddy, D. S.; Goud, B. S.; Rae, D. C.; Desiraju, G. R. *J. Chem. Soc., Perkin Trans. 2* **1994**, 2353−2360.

(9) Anthony, A.; Desiraju, G. R.; Kuduva, S. S.; Madhavi, N. N. L.; Nangia, A.; Thaimattam, R.; Thalladi, V. R. *Cryst. Eng.* **1998**, *1*, 1−18.

(10) Jetti, R. K. R.; Xue, F.; Mak, T. C. W.; Nangia, A. *Cryst. Eng.* **1999**, *2*, 215−224.

(11) Bosch, E.; Barnes, C. L. *Cryst. Growth Des.* **2002**, *2*, 299−302.

(12) Saha, B. K.; Jetti, R. K. R.; Reddy, L. S.; Aitipamula, S.; Nangia, A. *Cryst. Growth Des.* **2005**, *5*, 887−899.

(13) Hathwar, V. R.; Guru Row, T. N. *J. Phys. Chem. A* **2010**, *114*, 13434−13441.

(14) Solimannejad, M.; Malekani, M.; Alkorta, I. *J. Phys. Chem. A* **2010**, *114*, 12106−12111.

(15) Bui, T. T. T.; Dahaoui, S.; Lecomte, C.; Desiraju, G. R.; Espinosa, E. *Angew. Chem., Int. Ed.* **2009**, *48*, 3838−3841.

(16) Williams, D. E.; Hsu, L. Y. *Acta Crystallogr., Sect. A* **1985**, *41*, 296−301.

(17) Aubert, E.; Lebègue, S.; Marsman, M.; Bui, T. T. T.; Jelsch, C.; Dahaoui, S.; Espinosa, E.; Ángyán, J . G. *J. Phys. Chem. A* **2011**, *115*, 14484−14494.

(18) (a) Coppens, P. *X-ray Charge Densities and Chemical Bonding*; Oxford University Press: Oxford, U.K., 1997. (b) Koritsanszky, T. S.; Coppens, P. *Chem. Rev.* **2001**, *101*, 1583−1621. (c) Gatti, C., Macchi, P. *Modern Charge Density Analysis*; Springer: Berlin, 2012.

(19) (a) *CrysAlisPro CCD and CrisAlisPro RED*; Oxford Diffraction Ltd.: Yarnton, Oxfordshire, U.K., 2009. (b) Otwinowski, Z.; Minor, W. *Methods Enzymol.* **1997**, *276*, 307−326.
(20) DeTitta, G. T. *J. Appl. Crystallogr.* **1985**, *18*, 75−79.
(21) Blessing, R. H. *Crystallogr. Rev.* **1987**, *1*, 3−58.
(22) Altomare, A.; Cascarano, G.; Giacovazzo, C.; Guagliardi, A.; Burla, M. C.; Polidori, G.; Camalli, M. *J. Appl. Crystallogr.* **1994**, *27*, 435−436.
(23) Sheldrick, G. M. *Acta Crystallogr., Sect. A* **2008**, *64*, 112−122.
(24) Farrugia, L. J. WinGX (Version 1.80.05). *J. Appl. Crystallogr.* **1999**, *32*, 837−838.
(25) (a) MoPro: Jelsch, C.; Guillot, B.; Lagoutte, A.; Lecomte, C. *J. Appl. Crystallogr.* **2005**, *38*, 38−54. (b) MoProViewer: Guillot, B. *Acta Crystallogr., Sect. A* **2011**, *67*, C511−C512.
(26) Macrae, C. F.; Edgington, P. R.; McCabe, P.; Pidcock, E.; Shields, G. P.; Taylor, R.; Towler, M.; van de Streek, J. *J. Appl. Crystallogr.* **2006**, *39*, 453−457.
(27) (a) Kresse, G.; Hafner, J. *Phys. Rev. B* **1993**, *47*, 558−561. (b) Kresse, G.; Hafner, J. *J. Phys.: Condens. Matter* **1994**, *6*, 8245−8257. (c) Kresse, G.; Furthmüller, J. *Comput. Mater. Sci.* **1996**, *6*, 15−50. (d) Kresse, G.; Furthmüller, J. *Phys. Rev. B* **1996**, *54*, 11169−11186.
(28) (a) Blöchl, P. E. *Phys. Rev. B* **1994**, *50*, 17953. (b) Kresse, G.; Joubert, D. *Phys. Rev. B* **1999**, *59*, 1758−1775.
(29) Perdew, J. P.; Burke, K.; Ernzerhof, M. *J. Chem. Phys.* **1996**, *77*, 3865−3868.
(30) Frisch, M. J.; et al. *Gaussian 09*, revision C.01 (see the full reference in the Supporting Information).
(31) Keith, T. A.; Gristmill, T. K. *AIMAll (Version 12.06.03) Software*; Overland Park: KS, 2012; aim.tkgristmill.com.
(32) Hansen, N. K.; Coppens, P. *Acta Crystallogr., Sect. A* **1978**, *34*, 909−921.
(33) (a) Bendeif, E. E. Ph.D. Thesis; University of Nancy I: France, 2006. (b) Garcia, P. Ph.D. Thesis; University of Nancy I: *France*, 2007.
(34) Stewart, R. F.; Davidson, E. R.; Simpson, W. T. *J. Chem. Phys.* **1965**, *42*, 3175−3187.
(35) (a) Domagała, S.; Jelsch, C. *J. Appl. Crystallogr.* **2008**, *41*, 1140−1149. (b) Paul, A.; Kubicki, M.; Kubas, A.; Jelsch, C.; Fink, K.; Lecomte, C. *J. Phys. Chem. A* **2011**, *115*, 12941−12952.
(36) Hirshfeld, F. L. *Acta Crystallogr., Sect. A* **1976**, *32*, 239−244.
(37) (a) Bader, R. F. W. *Atoms in Molecules − A Quantum Theory*; Clarendon: Oxford, U.K., 1990. (b) Bader, R. F. W. *J. Phys. Chem. A* **1998**, *102*, 7314−7323. (c) Bader, R. F. W. *J. Phys. Chem. A* **2009**, *113*, 10391−10396.
(38) (a) Coppens, P. *X-ray Charge Densities and Chemical Bonding*; Oxford University Press: Oxford, U.K., 1997. (b) Koritsanszky, T. S.; Coppens, P. *Chem. Rev.* **2001**, *101*, 1583−1621.
(39) Bader, R. W. F.; Beddall, P. M. *J. Chem. Phys.* **1972**, *56*, 3320−3329.
(40) (a) Espinosa, E.; Molins, E.; Lecomte, C. *Chem. Phys. Lett.* **1998**, *285*, 170−173. (b) Espinosa, E.; Alkorta, I.; Rozas, I.; Elguero, J.; Molins, E. *Chem. Phys. Lett.* **2001**, *336*, 457−461.
(41) Abramov, Yu. A. *Acta Crystallogr., Sect. A* **1997**, *53*, 264−272.
(42) Brown, G. M.; Strydom, O. A. W. *Acta Crystallogr., Sect. B* **1974**, *30*, 801−804.
(43) Baharie, E.; Pawley, G. S. *Acta Crystallogr., Sect. A* **1979**, *35*, 233−235.
(44) Wójcik, G.; Toupet, L.; Gors, C.; Foulon, M. *Phys. Status Solidi A* **1995**, *147*, 99−109.
(45) Sakurai, T. *Acta Crystallogr.* **1962**, *15*, 1164−1173.
(46) Wójcik, G.; Rohleder, J. W. *Acta Phys. Pol., A* **1976**, *49*, 485.
(47) Betz, R.; Klüfers, P.; Mayer, P. *Acta Crystallogr., Sect. E* **2008**, *64*, o1921.
(48) Bondi, A. *J. Phys. Chem.* **1964**, *68*, 441−451.
(49) Reddy, C. M.; Kirchner, M. T.; Gundakaram, R. C.; Padmanabhan, K. A.; Desiraju, G. R. *Chem.-Eur. J.* **2006**, *12*, 2222−2234.
(50) (a) Das, D.; Banerjee, R.; Mondal, R.; Howard, J. A. K.; Boese, R.; Desiraju, G. R. *Chem. Commun.* **2006**, 555−557. (b) Taylor, R.; Macrae, C. F. *Acta Crystallogr., Sect. B* **2001**, *57*, 815−827. (c) Oswald, D. H.; Allan, D. R.; Motherwell, W. D. S.; Parsons, S. *Acta Crystallogr., Sect. B* **2005**, *61*, 69−79. (d) Gdaniec, M. *CrystEngComm* **2007**, *9*, 286−288.
(51) (a) Nobeli, I.; Price, S. L. *J. Phys. Chem. B* **1999**, *103*, 6448−6457. (b) Desiraju, G. R. *CrystEngComm* **2007**, *9*, 91−92.
(52) (a) Ermer, O. *Angew. Chem., Int. Ed. Engl.* **1994**, *33*, 471−476. (b) Brock, C. P.; Duncan, L. L. *Chem. Mater.* **1994**, *6*, 1307−1312.
(53) (a) Tsirelson, V. G.; Zou, P. F.; Tang, T. H.; Bader, R. F. W. *Acta Crystallogr., Sect. A* **1995**, *51*, 143−153. (b) Boese, R.; Boese, A. D.; Blaser, D.; Antipin, M. Yu.; Ellern, A.; Seppelt, K. *Angew. Chem., Int. Ed. Engl.* **1997**, *36*, 1489−1492.
(54) Espinosa, E.; Alkorta, I.; Elguero, J.; Molins, E. *J. Chem. Phys.* **2002**, *117*, 5529−5542.
(55) Dominiak, P. M.; Espinosa, E.; Ángyán, J. G. In *Modern Charge Density Analysis*; Gatti, C., Macchi, P., Eds.; Springer: Berlin, 2012; Chapter 11, pp 387−434.
(56) (a) Matta, C. F.; Castillo, N.; Boyd, R. J. *J. Phys. Chem. B* **2006**, *110*, 563−578. (b) Lyssenko, K. A.; Borissova, A. O.; Burlov, A. S.; Vasilchenko, I. S.; Garnovskii, A. D.; Minkin, V. I.; Antipin, M. Y. *Mendeleev Commun.* **2007**, *14*, 164−166. (c) Nelyubina, Y. V.; Antipin, M. Y.; Lyssenko, K. A. *J. Phys. Chem. A* **2009**, *113*, 3615−3620. (d) Lyssenko, K. A.; Barzilovich, P. Y.; Aldoshin, S. M.; Antipin, M. Y.; Dobrovolsky, Y. A. *Mendeleev Commun.* **2008**, *18*, 312−314. (e) Nelyubina, Y. V.; Troyanov, S. I.; Antipin, M. Y.; Lyssenko, K. A. *J. Phys. Chem. A* **2009**, *113*, 5151−5156. (f) Lyssenko, K. A.; Nelubina, Y. V.; Safronov, D. V.; Haustova, O. I.; Kostyanovsky, R. G.; Lenev, D. A.; Antipin, M. Y. *Mendeleev Commun.* **2005**, *15*, 32−36. (g) Korlyukov, A. A.; Lyssenko, K. A.; Antipin, M. Y.; Grebneva, E. A.; Albanov, A. I.; Trofimova, O. M.; Zel'bst, E. A.; Voronkov, M. G. *J. Organomet. Chem.* **2009**, *694*, 607−615. (h) Nelyubina, Y. V.; Lyssenko, K. A.; Kostyanovsky, R. G.; Bakulin, D. A.; Antipin, M. Y. *Mendeleev Commun.* **2008**, *18*, 29−31. (i) Nelyubina, Y. V.; Lyssenko, K. A.; Golovanov, D. G.; Antipin, M. Y. *CrystEngComm* **2007**, *9*, 991−996. (j) Nelyubina, Y. V.; Antipin, M. Y.; Lyssenko, K. A. *J. Phys. Chem. A* **2007**, *111*, 1091−1095. (k) Borissova, A. O.; Antipin, M. Y.; Perekalin, D. S.; Lyssenko, K. A. *CrystEngComm* **2008**, *10*, 827−832. (l) Lyssenko, K. A.; Korlyukov, A. A.; Golovanov, D. G.; Ketkov, S. Y.; Antipin, M. Y. *J. Phys. Chem. A* **2006**, *110*, 6545−6551. (m) Borissova, A. O.; Korlyukov, A. A.; Antipin, M. Y.; Lyssenko, K. A. *J. Phys. Chem. A* **2008**, *112*, 11519−11522. (n) Peganova, T. A.; Valyaeva, A.; Kalsin, A. M.; Petrovskii, P. V.; Borissova, A. O.; Lyssenko, K. A.; Ustynyuk, N. A. *Organometallics* **2009**, *10*, 3021−3028. (o) Puntus, L. N.; Lyssenko, K. A.; Antipin, M. Y.; Büunzli, J. C. G. *Inorg. Chem.* **2008**, *47*, 11095−11107. (p) Bushmarinov, I. S.; Antipin, M. Y.; Akhmetova, V. R.; Nadyrgulova, G. R.; Lyssenko, K. A. *J. Phys. Chem. A* **2008**, *112*, 5017−5023.
(57) (a) Bianchi, R.; Forni, A.; Pilati, T. *Chem.-Eur. J.* **2003**, *9*, 1631−1638. (b) Bianchi, R.; Forni, A.; Pilati, T. *Acta Crystallogr., Sect. B* **2004**, *60*, 559−568. (c) Forni, A. *J. Phys. Chem. A* **2009**, *113*, 3403−3412. (d) Nelyubina, Y. V.; Antipin, M. Y.; Dunin, D. S.; Kotov, Y. U.; Lyssenko, K. A. *Chem. Commun.* **2010**, *46*, 5325−5327.
(58) Awwadi, F. F.; Willet, R. D.; Peterson, K. A.; Twamley, B. *Chem.-Eur. J.* **2006**, *12*, 8952.
(59) (a) Clark, T.; Hennemann, M.; Murray, J. S.; Politzer, P. *J. Mol. Model.* **2007**, *13*, 291−296. (b) Murray, J. S.; Lane, P.; Polizer, P. *J. Mol. Model.* **2009**, *15*, 723−729.
(60) (a) Amezaga, N. J. M.; Pamies, S.; Peruchena, N.; Sosa, G. L. *J. Phys. Chem. A* **2010**, *114*, 552−562. (b) Eskandari, K.; Zariny, H. *Chem. Phys. Lett.* **2010**, *492*, 9−13. (c) Zhang, X.; Zeng, Y.; Li, X; Meng, L.; Zheng, S. *Struct. Chem.* **2011**, *22*, 567−576.
(61) (a) Gavezzotti, A. *J. Phys. Chem. B* **2003**, *107*, 2344−2353. (b) Gavezzotti, A. *OPiX*; University of Milano: Italy, 2003.
(62) Abboud, M.; Kadimi, A.; Mamane, V.; Aubert, E. *Acta Crystallogr., Sect. C* **2010**, *66*, o381−384.